POLITECNICO DI MILANO

Scuola di Ingegneria Industriale e dell'Informazione

Corso di Laurea Magistrale in Material Engineering and Nanotechnology

Development of a novel Fe-based wear and corrosion protection coating applied via High Velocity Air-Fuel (HVAF)

Supervisor: Prof. Marco Ormellese

External supervisor: Prof. Kirsten Bobzin

Candidate:

Mohsen Bahrami

Matr. 863755

Academic Year 2017-2018

D E C LA R A T IO N

I hereby declare that this material, which I now submit for the assessment on the program of study leading to the master degree, is entirely my own work. To the best of my knowledge, the results presented in this thesis originated from the presented study, except where references have been made. No part of this thesis has been submitted for a degree at any other institution.

Singed:

Mohsen Bahrami

Student. No. 863755

December 2018

TABLE OF CONTENTS

List of figures

List of tables

Acknowledgement

My first vote of thanks must go to my kind supervisor Professor Marco Ormellese who supported and supervised me unstintingly. I am greatly indebted to him for giving special attention and support to my work. I am privileged to have worked with him. I owe him much gratitude.

I am grateful to Professor K. Bobzin for initially selecting me from the department of materials engineering of POLIMI for doing my master thesis in IOT institute of Aachen.

I would like to express my sincere thanks to Mr. Jan Summer, research associate of thermal spray group, for his unceasing enthusiasm, interest, constructive criticism and practical hand on assistance with the HVAF thermal spray system. His expertise, availability to discuss ideas and willingness to share his knowledge were instrumental in the completion of this thesis.

My honest gratefulness is extended to my family, especially my dear mother and beloved father who have given their utmost support throughout my life so far. They have inspired me whole-heartedly since my childhood to progress in my educational career.

Astratto

L'obiettivo di questa ricerca è quello di studiare il potenziale di rivestimenti nobili economici a base di Fe per applicazioni su grandi superfici, in particolare gli essiccatori rotativi per la produzione di carta. Questi cilindri rotanti dovrebbero avere un alto livello di resistenza alla corrosione e all'usura per garantire un periodo di funzionamento più lungo. I rivestimenti resistenti all'usura e alla corrosione a base di Fe applicati grazie a tecniche di termo spruzzatura sono in via di sviluppo come alternativa economica per i rivestimenti a base di Ni-WC.

In questo studio, come processo di deposizione è stato utilizzato un sistema di termo spruzzatura che utilizza come combustibile aria ad alta velocità (HVAF-High Velocity Air Fuel) piuttosto che la tecnica Wire-Arc-Spraying (WAS), attualmente utilizzata per proteggere i cilindri delle macchine per la produzione della carta. Per fare ciò, sono state applicate polveri di FeCrB a diversa granulometria (-32+11μm e -20+3μm) utilizzando due diverse velocità di alimentazione della polvere (ṁ=40g/min e ṁ=200g/min). La microstruttura, la topografia e le fasi dei rivestimenti sono stati analizzati rispettivamente con microscopio ottico, microscopio elettronico a scansione (SEM), microscopio confocale a scansione laser (CLSM) e diffrazione dei raggi X (XRD). Sono stati eseguiti test di indentazione e di durezza Vickers per determinare rispettivamente la tenacità alla frattura e la microdurezza. Le proprietà di usura e corrosione sono state analizzate utilizzando rispettivamente i test di polarizzazione elettrochimica e pin-on-disc (POD). In definitiva, i risultati sono stati confrontati con il rivestimento industriale FeCrBSiMnC applicato con tecnica WAS e sigillato che è stato preso come riferimento. La tecnica WAS è infatti una tecnica molto comune a livello industriale per ricoprire cilindri essiccatori. I rivestimenti HVAF hanno presentato una microstruttura senza crepe, più densa e con un contenuto di ossidi inferiore rispetto al rivestimento prodotto con WAS. Grazie a queste caratteristiche unite alle migliori proprietà meccaniche dei rivestimenti HVAF, la resistenza all'usura e alla corrosione è risultata superiore a quella del sistema di rivestimento WAS.

Abstract

The aim of this research is to investigate the potential of noble cost-efficient Fe-based coatings for large area applications, especially rotary dryers of paper machines. These rotary cylinders supposed to have a high level of corrosion and wear resistance to ensure a longer operating period. Thermally sprayed Fe-based wear and corrosion resistance coatings are a developing trend as cost-effective alternative for thermally sprayed Ni- and WC-based coatings.

In this study, a High Velocity Air-Fuel (HVAF) thermal spray system was used as a deposition process, rather than Wire-Arc-Spraying (WAS) technique, which is currently used to protect cylinders of paper manufacturing machines. To do so, different powder fractions (-32+11µm and -20+3µm) of FeCrB feedstock material were applied with two different powder feed rates (ṁ=40g/min and ṁ=200g/min). Microstructure details, topography and phase composition of coatings were analyzed using light microscope, scanning electron microscopy (SEM), confocal laser scanning microscope (CLSM) and x-ray diffraction (XRD) respectively. The indentation and Vickers tests were carried out to determine the fracture toughness and microhardness of sprayed coatings. In addition, the wear and corrosion properties were investigated using pin-on-disc (POD) and electrochemical polarization tests respectively. Ultimately, the results were compared to the industrially established sealed WAS FeCrBSiMnC coating as a reference, which is a common technique to coat the dryer cylinders. Such HVAF coatings exhibited crack-free and denser microstructure with lower oxide content compared to the coating manufactured with WAS. Due to the lower amount of porosity and oxide as well as better mechanical properties of sprayed HVAF coatings, both wear and corrosion resistance of the HVAF coatings were superior compared to that of the WAS coating system.

Chapter 1

Introduction

1.1 Background and approach

Nowadays, the main focus of research in the field of thermally sprayed protection coatings is not only to develop high performance coatings but also to optimize environmental and economic factors such as raw materials and post-processing costs. For this reason, Fe-based alloys have recently attracted significant interest as feedstock materials for the wear-and corrosion-resistant coatings applications. Firstly, Fe as the main constituent of these alloys is relatively cost-efficient in compare to basis elements of hardfacing alloys such as Co [1, 2]. Secondly, typical alloying elements such as Ni and Co are toxic, allergenic and hazardous for human health in the form of powder and even solid materials (include coated parts) [3-5]. Recent literatures, have utilized Fe-Cr-C [6-12] and Fe-Cr-B(-C) [7-11, 13] as the Fe-based protective coating system, either in (nano) crystalline [7-12] , glassy [8, 9, 14], or composite (glass + nanocrystals) [13] form, deposited by cladding [11, 12, 15] or by thermal spraying [6, 8-10]. Among the thermal spraying techniques, WAS [16-20], Air Plasma Spray (APS) [21-23], High Velocity Oxy-Fuel (HVOF) [7, 9, 20, 24-26] and HVAF [24, 25, 27-30] have been employed for coating of valves, pistons, impellers, shafts and journal bearings, automatic machine parts, cylinders and rolls, etc. The purpose of this project is to protect the rotary dryers of paper machines, which are exposed to combined load of wear and corrosion. The typical protective coatings system for these dryers are the WAS spray of Fe-based feedstock materials and cemented carbides applied by the HVOF [31]. The Fe-based WAS coatings have a cost-efficiency and high achievable wire feed rates. In contrast, the produced coatings are thick and rough which requires time-consuming post-production processes and leads to undesired high thermal insulation. Moreover, the microstructure of the WAS coatings is mostly pours which is not

appropriate for corrosion and tribological applications. To further protection of WAS coatings against corrosion, porosities can be sealed with epoxy resin [32, 33]. On the other side, the HVOF process is able to produce thin and smooth cemented carbide coatings with high corrosion and wear resistance. However, the deposition rates in this process are usually lower than WAS technique. Furthermore, the production costs are typically high due to the expensive raw material e.g. WC-Co, Cr_3C_2/NiCr [31, 34].

The solution approach is to get the bests of both the WAS and the HVOF techniques. Number of studies have confirmed this fact that the HVAF process, which is the modification of the HVOF, has some valuable advantages respect to the other thermal spraying techniques specially WAS and HVOF, include denser microstructure, higher deposition rate, lower process and particle in-flight temperature, thinner coatings and shorter process time [24, 35-38].

The study presented in this paper is specifically concerned with HVAF spray of the novel FeCrB alloy system to produce dense and crack-free coatings with powder feed rates of $\dot{m}$=40g/min and $\dot{m}$=200g/min. Furthermore, in order to achieve more uniform molten particles and decrease a residual stress, the finer powder fraction of -20+3µm is used besides coarse one -32+15µm. Moreover, thinner and near-net-shape coatings can be achieved with the fine powder fraction. Thinner coatings have positive effects on saving feedstock material, decreasing the production time as well as energy savings due to the reduction of the thermal insulation effect of the coatings. Thus, the influence of a coating thickness reduction below d_{ct}=150µm on the corrosion and wear behavior is also investigated. Therefore, the present research aims to provide an assessment of the tribological, mechanical and corrosion properties of HVAF-sprayed FeCrB coatings with two different powder feed rates and powder fractions, and comparison of the results with the sealed WAS sprayed FeCrBSiMnC reference coating system.

1.2 Thesis Outline

This thesis comprises six chapters and two appendices. The remainder of this chapter gives a brief description of surface engineering. Chapter 2 describes about thermal spray coatings, their different techniques and suitable materials for these systems. Chapter 3

presents the raw materials, theoretical background of the tests, the experimental equipment and procedures, characterization and optimization of the coatings, and the evaluation methods of the results. Chapter 4 discusses the experimental performance and results. Finally, chapter 5 and 6 include the conclusions of the thesis, recommendations for further work as well as thesis references respectively.

1.3 Surface Engineering

Surface engineering is a valuable tool in achieving better environmental sustainability and reduced life-cycle costs. As described by Halling [39], "Surface engineering can be defined as the branch of science that deals with methods for achieving the desired surface requirements and their behavior in service for engineering components". Engineering components have specific functions that must be performed under different conditions in aggressive environments. Generally, surface engineering involves either microstructural modification or compositional changes or both. Improving the wear-, oxidation-, and corrosion-resistances, friction coefficients, mechanical properties, thermal insulation, aesthetic appearance and mechanical properties are some of desired achievements of surface engineering. Surface treatments that cause microstructural modifications in the bulk material consist of mechanical treatments or heating and cooling through induction, laser, flame and electron beam processes. On the other hand, compositional changes originated by diverse techniques such as carburizing, nitriding, carbonitriding, nitrocarburizing, boriding, aluminizing, chromizing and siliconizing. Among all the compositional surface engineering processes, coating, which is simply defined as an artificial deposition of single or multilayered materials on the substrate, is one of the most economical and convenient treatments used to obtain some required technical or decorative properties or to protect the material from chemical and physical interactions with its surrounded environment [40, 41].

Chapter 2

Thermal Spray Coatings

Thermal spray technology is an established industrial surfacing method to achieve a thick or thin coating and improve the performance of substrate or component by means of functional surfaces. Fig.1 shows the typical working principle of thermal spray techniques in which a heat/energy source melts the feedstock materials in form of powder, wire, rod or cord. Afterward, process gases, along with air in some cases, accelerate the molten or semi-molten material onto a prepared substrate. The accelerated particles strike the surface of a substrate, flatten and form thin platelets called splats that adhere to the asperities on the substrate surface. After cooling down of splats they build up splat by splat a lamellar-structured coating [34, 42].

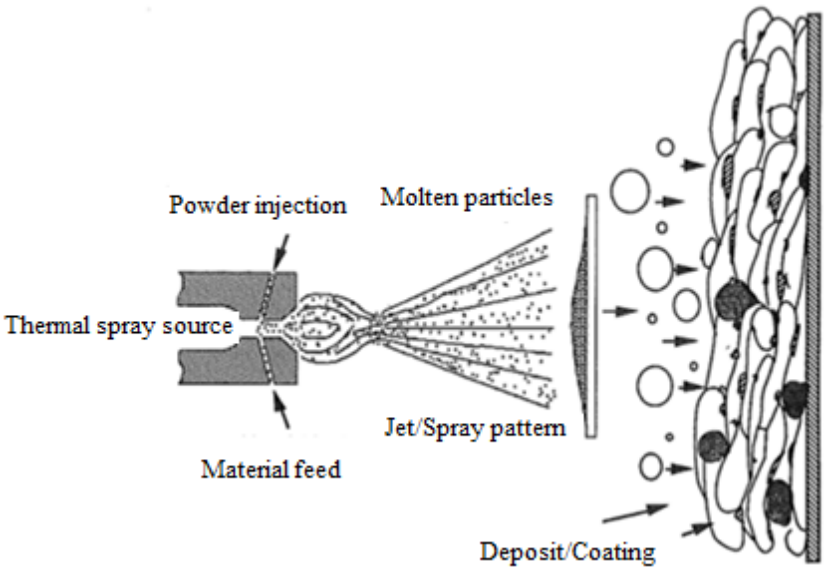

Figure 1: Schematic diagram of thermal spray processes [43]

Fig.2 depicts the typical lamellar thermal spray coatings microstructure containing unmolten particles, oxides, porosity, and debris. Voids can happen if the growing deposit traps air. Unmolten particles may simply be embedded in the accumulating deposit. Oxidized particles can be produced by overheating of particles in the spray jet [44].

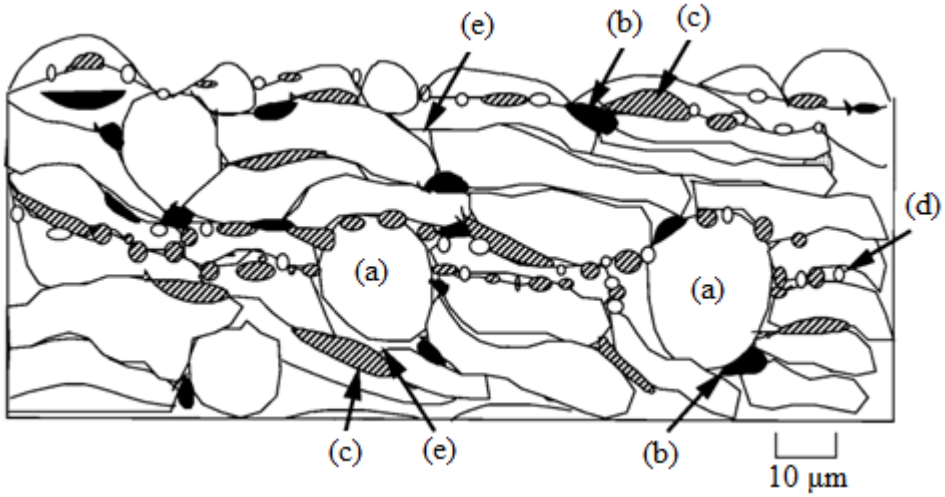

Figure 2: Typical thermal spray coatings microstructure (a) unmolten particles, (b) oxides, (c) debris, (d) fine particles, (e) porosity [44]

Thermal spray coating processes have variety advantages respect to other techniques. The first is versatility in materials. Almost any metal, ceramic or plastic, in general any material which melts without decomposing can be used in thermal spray processes [43]. The second is formation of coating with minimum heating of the substrate. Substrate temperature seldom exceeds 250°C. Therefore, pre- or post-heat treatment as well as substrate distortion are minimum. Another advantage is that in most cases, recoating the damaged surface would not change the properties of coating[45]. In addition, with thermal spray process wide range of thickness can be achieved (from 0.001 to more than 1 inch). The cost reduction is another benefit since the coating often lasts longer than the original material used, also the cost of component repairing is less than new one[46].

The main achievement of thermal spray coating technologies is providing a protective surface with properties of wear resistance, corrosion resistance, thermal insulation and electrically conductive in several application fields such as aerospace, automotive, power and chemical industries, to name but a few [43, 45, 47, 48]. As listed in Fig.3, thermal spray coating deposition technologies are widely used to reduce the cost, improve engineering performance and/or increase component life.

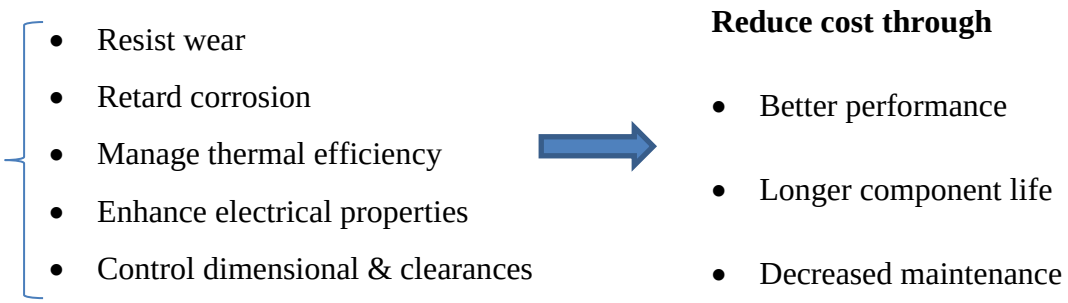

Figure 3: List of thermal spray technique achievements

2.1 Thermal Spray Techniques

The thermal spray family consists of variety techniques, which provide different properties to the resulting coating. As it presented in Fig.4 [34] thermal spray processes are usually classified based on the type of energy source utilized for melting feedstock materials. The most typical energy sources in thermal spray are divided to five groups in which the thermal and/or kinetic energy obtained from [34]:

1- Combustion of gases; typically hydrocarbon or hydrogen
2- Molten liquid
3- Electric discharges; electric arcs or ionized plasma gases
4- Purely kinetic energy sources
5- High-power laser beams

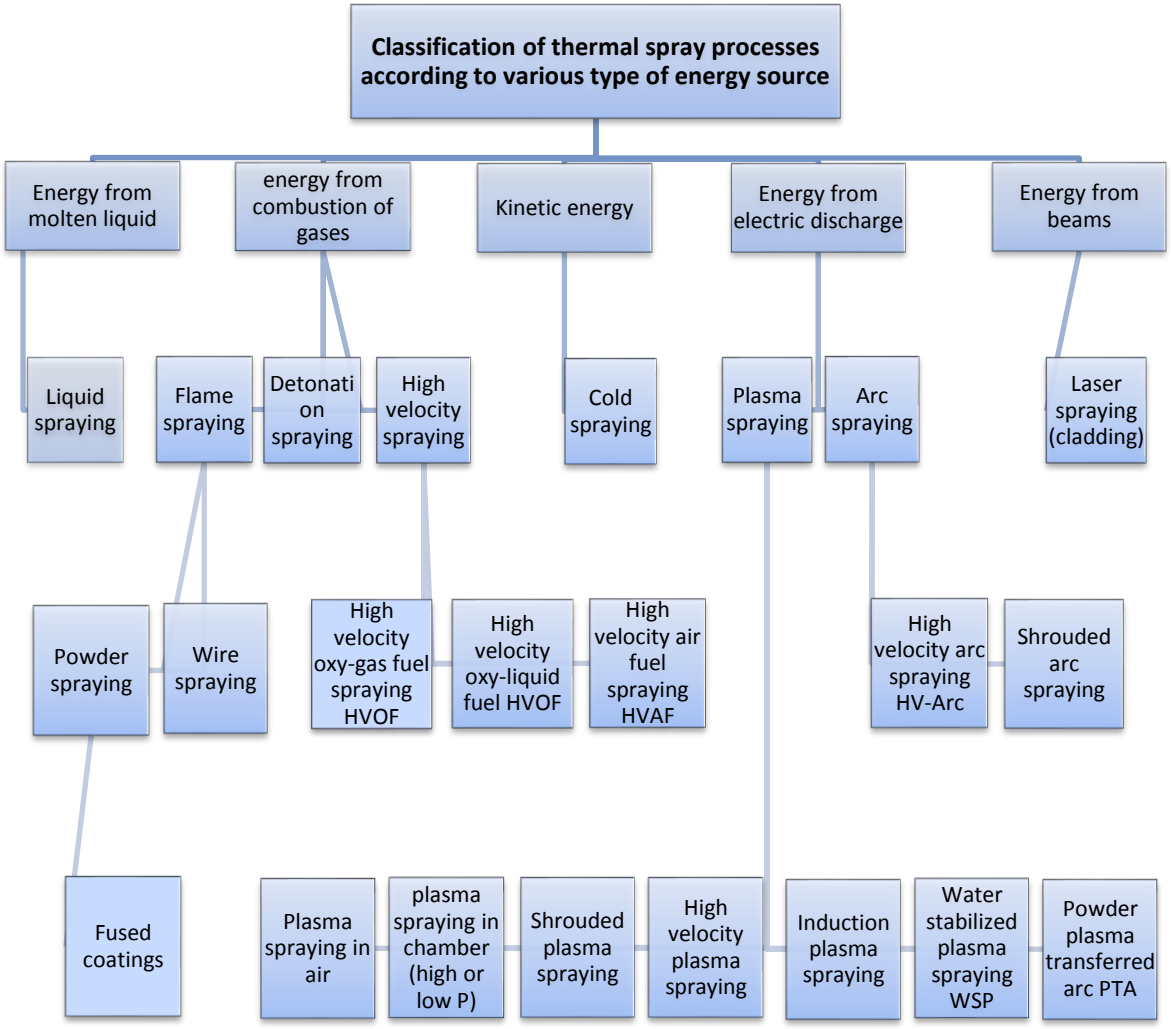

Figure 4: Classification of thermal spray coating processes according to the type of energy source used in the process [34]

Further classification of thermal spray processes can be according to the spray gun design, type of used feedstock material, type of fuel (gas or liquid), type of deposition atmosphere (e.g. atmospheric, low/high pressure, inert gas and under water), type of oxidizer in combustion, etc. The most prevalent thermal spray techniques that are available commercially includes Flame Spray Powder/Wire, Detonation, High Velocity Oxygen Fuel (HVOF), and High Velocity Air Fuel (HVAF), which these processes associated with combustion. Plasma and Wire Arc are processes in which consumable material melts by means of electric energy. The detonation, HVOF and HVAF techniques result in high

strength bond and extremely dense microstructure. Plasma coatings, which can be either Low-Pressure Plasma Spray (LPPS) or Vacuum Plasma Spray (VPS), are also known to have high bond strength as well as relatively dense oxide-free microstructures. Cold Spray is another process which is more based on high velocity and kinetic energy rather than thermal energy [49].

Table1 presents not only some important numerical data (very generalized) of different thermal spray techniques but also compares them together. It is worth underlining that all numbers and values presented in the table are highly sensitive to material, parameter, and process/equipment and therefore can be useful only for general comparison of different processes. The key point to select and use of optimal thermal spray technique successfully, is understanding the technological and economical advantages and limitations of different processes [34, 49].

Spray Process	Temp.[g] (ºC)	Particle velocity (m s^{-1})	Oxide cont.[d] (%)	Porosity (%)	Adhesion [c] (MPa)	Spray rate (kg h^{-1})	Coating thickness (mm)	Relative cost[a]
Flame	3000	40	10-15	10-15	8	2-6	0.1-15	1
Electric arc	4000	100	10-20	10	12	10-25	0.1-15	2
HVOF	3000	600-800	1-5	1-2	>70	2-8	0.1-2	3
HVAF	2000-3000	600-1200[f]	***[e]	0-0.2	>70	Hard metals: 2-30; metals: 2-23[b]	0.1-12	2
Detonation	4000	800-1200	1-5	1-2	>70	0.5-2	0.05-0.3	4
APS	12000	200-400	1-3	1-5	10-70	2-10	0.1-1	4
LPPS/VPS	12000	400-600	0	<0.5	>70	2-6	0.1-1	5

Table 1: Comparison of characteristics of coatings deposited by different thermal spray processes [34, 49, 50]

[a] Investment cost of process
[b] Depends on gun type; M2 AC-HVAF spray gun; M3 supersonic spray gun
[c] Depends on deposit material
[d] Oxide content in metallic deposits
[e] Oxide content is approximately 1.5–2 times the oxide content of the feedstock
[f] Depends on equipment type; e.g., M2 AC-HVAF, 600–700 m s^{-1}; M3 SAP, 800–1200 m s^{-1}
[g] Temperature of the heat source

Since the focus of this project is to offer a protective coating in term of corrosion and wear for the paper machine industry, the most common coating techniques for this purpose are WAS, HVOF and HVAF processes that are investigated in details in the following part.

2.1.1 Wire-Arc-Spray

Wire arc spraying (WAS) is an inexpensive technique of thermal spraying which has become popular due to the low operating and equipment costs as well as high material and energy efficiencies. Fig.5 schematically shows the WAS process and the spraying system.[50, 51]

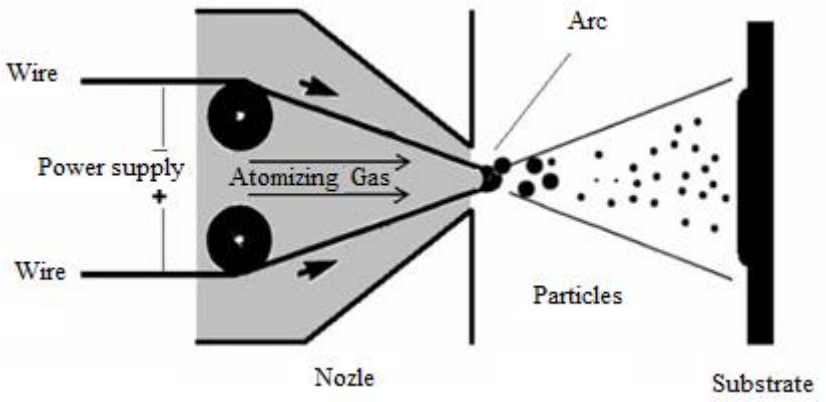

Figure 5: Schematic presentation of the WAS process

The industrial wires that are usually made of electrically conductive materials such as Aluminum, Zinc, Stainless Steel, and Copper, are continuously fed into the gun. By applying the electric voltage in range of 40 V, arc produces in the gap between the wire tips. After heating the wire tips with electric arc, a thin layer of molten material is produced. A high-velocity atomizing gas flow (air or nitrogen) between the wires and across the arc constantly, removes the molten material from the wire tips, breaks down the larger droplets into smaller ones (secondary atomization process), and moves them toward the substrate. The molten droplets deposit on the substrate one over another and then they solidify and form a coating layer. It is possible to spray a wide range of metals, alloys and metal matrix composites (MMCs) to various low melting point substrates.[52, 53] The produced arc spray coatings usually have a greater porosity and lower adhesion strength than coatings obtained from other thermal spray techniques, making them of relatively poorer quality. However, following advantages make the WAS as an attractive process in industry:[54, 55]

- Cost efficient: the simple design of equipment, the low cost of electrical power and producing wires
- On-site applications: due to the light weight and portable design
- Safe process: use of non-flammable gases
- Low temperature of atomizing gas causes reduction of heat transfer rate to the substrate; prevents damage, distortion and metallurgical changes of substrate surface.
- Energy-efficient process: complete melting of input materials
- High deposition efficiency (mass ratio of coated material to fed material): be comparable and, in some cases, better than that of other thermal spray processes.

Besides poor quality of the WAS coatings, another disadvantage is the lack of control over the size of the produced particles. Despite the most of the thermal spray processes in which the molten droplet sizes are determined by solid particle sizes in the fed powder, in wire arc spray the molten droplet sizes are determined by the operating parameters. Since the particle size controls dynamic and thermal behavior within the spray and spreading behavior during deposition, this lack of control limits the ability to adjust coating characteristics according to the wide range of industrial requirements, thereby narrowing the range of wire-arc applications.

Arc sprayed coatings are used widely for corrosion protection in the automobile industry, marine applications (ship hulls, decks, or platforms) or for infrastructure maintenance (coatings of bridge structures, storage tanks). Other common anticorrosion application areas are offshore oil platforms, fences, underground pipes, electric rolled welded (ERW) tube manufacture, multi-void aluminum tube manufacture, LPG cylinders [56, 57]. The most important parameters which affect the microstructure of produced coatings in the WAS systems include [58-60]:

- Feed material as a wire: The variety range of materials being used as a wire such as aluminum, copper, stainless steel, tin, titanium, zinc, metal alloys and metallic composites. In addition, for non-conductive materials, cored wires are used, in which carbide, nitride, or cermet are wrapped inside and electric conductive layer cover them as an outer layer.
- The atomizing gas: In industrial applications, many atomizing gases are used such as dry-air, nitrogen and argon. In order to reduce oxide content of coating, lower amount of oxygen is preferred in the mixture of gas.

- Upstream pressure of atomizing gas: By means of upstream pressure is it possible to determine the volume-flow-rate and gas velocity. The velocity of atomizing gas directly affects the velocity of deposited droplets.
- Applied voltage: With the aim of applied voltage, the arc input power and the rate of heating and melting of wires can be controlled.
- Geometry of torch, the diameter of wires, feed mechanism for the wires

Furthermore, there are other factors that are not controlled by spraying system such as state of the ambient gas (e.g. moisture content) and state of substrate (e.g. temperature and roughness).

2.1.2 High Velocity Oxy-Fuel

The High Velocity Oxy-Fuel (HVOF) thermal spray is another type of combustion spray technique. The heating method is still the same as for flame spray; using the chemical energy of combusting fuel gases to generate heat, except that the HVOF utilizes a much higher velocity of the spray stream and uses powder as the coating material besides the wire or rod [61]. The purpose of the HVOF process is transferring of both thermal and kinetic energy to powder particles in an efficient way. This energy is provided by a combustion of gases mixture. A typical HVOF thermal spray system consists of following units: a gas supply, flow meter, powder feed and gun [62]. Fig.6 shows a schematic view of the HVOF process. The HVOF guns have an air- or water-cooled combustion chamber. The combustion fuel gas (hydrogen, propane, or propylene) and oxygen are fed to the spray gun together with the powder materials. The combustion of gases will produce high temperature and pressure in the spray gun. The burning gas mixture will accelerated to supersonic speeds through the nozzle, and the spray powder is ejected to the hot gas stream. Then the hot gas stream heats and accelerates the spray powder and projects them into the substrate. The bonding type is usually mechanical bonding between the coating and the substrate [43, 63, 64].

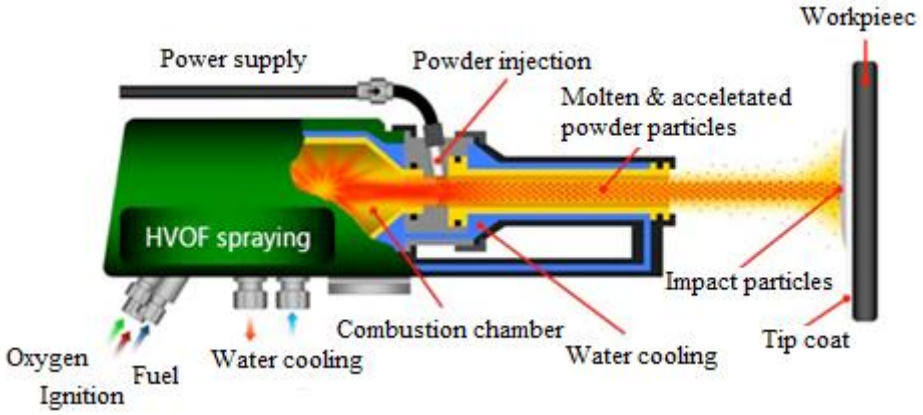

Figure 6: Schematic presentation of a HVOF process [65]

The gas velocity, which is generated by HVOF, is much higher in compare of conventional flame or plasma spray that resulted to increase of particle velocity, corresponds to increase of coating density and adhesion. On the other hand, the average of particles temperature in the HVOF is lower than plasma spray, reduces the degree of particle melting and oxidation. The benefit of high particle impact velocities is that despite the lower average particle temperatures, high coating densities are still achieved because of particles deformation and conversion of kinetic energy into thermal energy, which further helps in achieving dense coatings [43].

The HVOF technique is mostly used to deposit dense, hard and abrasion resistant coatings where adhesion is the main concern such as WC/Co or Cr_2C_3/NiCr, as well as metallic coatings with little or no oxidation. In particular, this technology is employed in the automotive, aerospace and chemical industries to produce coatings with high resistance to wear, thermal loads or corrosion. In addition, it is used in the textile and paper machinery which can be an interesting replacement to the galvanic technique with high environmental impact [43, 66, 67]. Another characteristic of the HVOF process is some control of residual stress. Generation of high pressure in the combustion chamber and high velocity impact produce compressive stress in the coatings so called “peening stress” which is useful for the function of most coatings. This control over residual stress allows significantly greater thicknesses to be applied compared to the plasma process [66, 68]. The typical microstructure of the HVOF coatings includes inter-lamellar boundaries, some un-molten particles, pores, oxides and inclusions [69].

2.1.3 High Velocity Air-Fuel

The High-Velocity Air Fuel (HVAF) technique is a relatively new method in the family of thermal spray processes. This process is a modified version of HVOF with use of air instead of oxygen, higher deposition rate and lower particle in-flight temperatures [70]. The mechanism of coating deposition is almost same as HVOF (Fig.7); first of all compressed air and a fuel gas (propane, propylene, or natural gas) are pre-mixed before entering the combustion chamber. After heating of ceramic wall of chamber the ignition occurs with help of an electric spark plug and combustion takes place. After that, the powder is injected with N_2 as a carrier gas into a nozzle and entrained by a hot supersonic gas stream. Fuel can also added to further increase of in-flight particle velocity and temperature. The solid powder particles are heated and accelerated to extreme velocities. Subsequent to impact of particles with the substrate, their kinetic energy is converted into thermal energy which further heats the particles and helps them to melt or deform sufficiently to deposit on the surface [71-73].

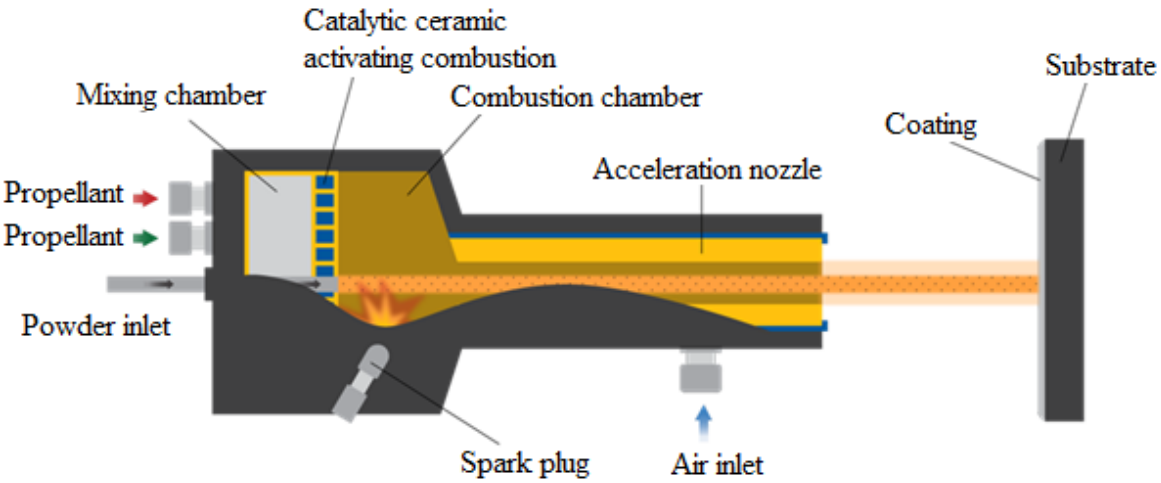

Figure 7: Schematic presentation of a HVAF process

The essential parameters, which can control the combustion process, consist of type of fuels, length and diameter of nozzles, amount and concentration of injected gas. Furthermore, the feedstock material characteristics such as chemical composition, particle size and distribution as well as morphology will affect the temperature and velocity of in-flight particles. The velocity of produced jet stream in the HVAF process is about 1400 m/s which accelerates particles up to 1100-1200 m/s. The high-speed particles not only provide a good adhesion strength between coating and substrate but also establish a dense coating. The temperature of HVAF flame is less than 1950°C that heats up the temperature of in-flight

particles around 1500°C [74] . In the standard HVAF spraying condition, the total oxygen content can be controlled below 1 wt.% due to the low heat input. In addition, relatively low process temperature assists spraying of sensitive materials to the temperature and oxidation such as materials consist of Cr or/and Al [43]. The bond strength of thermal spray coatings which has been reported by ASTM C633 is about 80 MPa, whereas this value for the HVAF coatings is up to 200 MPa [75]. The deposition efficiency (DE) of HVAF process has been reported in range of 58-65% for metal powders and 50-75% for carbide powders, which is fairly high compared to the other thermal spray processes. It is possible to increase the DE with optimization of both process parameters and feedstock material characteristics (e.g. optimal particle size with narrow distribution) [43]. In summary, the HVAF produced coatings are compact and dense, consist of lamellar structure which embedded with a few solid particles as well as minimal voids and pores at the surface and inter-lamellar particle boundaries [76].

2.2 Comparison of HVAF and HVOF Method

The HVAF technique provides significant advantages in terms of cost and coating properties. In this part, these advantages will be studied from different point of view.

- As mentioned before, the main difference of the HVOF and the HVAF techniques is replacing pure oxygen with the air in the HVAF, which reduces the in-situ oxidation significantly during spraying and decarburization effect after spraying [70, 77, 78].

- Combustion Temperature: The combustion temperature in oxygen-fuel mixtures is typically 1000°C higher than in air-fuel combustion. In the HVOF process, the combustion temperature may exceed metal boiling temperature; meanwhile, the lower combustion temperature of the HVAF is ideal for the gradual heating of the feedstock particles of metals and cemented carbides to or slightly above the metals' melting temperature. In addition, the initial oxygen content in the combustion gas mixture of the HVAF process is 5-fold lower compared to any HVOF process. These two factors prevent the oxidation of metals and oxidation/thermal deterioration of carbides. Moreover, they lead to keep the original ductility of the powder feedstock material in the applied coating. Another influence of lower combustion temperature

in the HVAF is ability to use chambers for long time and soft heating which provides better heat transfer and leads to the higher energy efficiency of the HVAF [79].

- The coatings produced by the HVAF process have a higher in-flight particles velocity (M2 ™, Unique coat, 700 m/s) and lower in-flight particle temperature (1900 °C) compared to those values for the HVOF process (JP-5000™, Diamond Jet, ≈600 m/s and 2200 °C). These features lead to create denser coatings with less porosity, higher level of compressive residual stress as well as minimal feedstock phase transformation [81 ,80 ,77].

- The HVAF spraying technique is less expensive with respect to the HVOF, therefore is more appropriate for the scale-up productions[24].

- In the HVAF deposition technique, the spray rate and deposition efficiency are 5-6 times and 20-30% higher than any HVOF system respectively. As a result, by means of the HVAF system it is possible to gain 50% cost advantage [79].

2.3 Coating Materials

There are a large number of modern coating materials available and suitable for thermal spray technology. In fact, any material that has a well-known melting point and can be heated without decomposed or evaporated is a candidate for coating material in the thermal spray process. These materials may be classified into three main groups [49, 82, 83]:

- **Single-phase materials**

Metals: Most pure metals and metal alloys have been thermally sprayed. Types of materials include, but are not limited to cobalt-based (Setllites and Tribaloys), nickel-based (Inconel 625), zinc, aluminum, tungsten, stainless steels, and NiCrBSi (self-fluxing) alloys. Similarity of sprayed alloys to many substrate metals, their high strength, and their corrosion, wear and/or oxidation resistance are some advantages of these materials.

Ceramics: Most of ceramics can be thermally sprayed including metallic oxides (Al_2O_3, stabilized ZrO_2, TiO_2); carbides (Cr_3C_2, TiC, WC, SiC), nitrides (TiN and Si3N4); and Spinels or perovskites (Mullite and 1-2-3-type superconducting oxides). Sprayed deposits of

ceramics typically utilized to provide thermal protection, wear and corrosion resistance and electrical insulation. In addition, the most suitable technique for thermal spraying of ceramics is plasma spraying thanks to its high jet temperatures.

Intermetallics: Most of intermetallics are very sensitive to high temperature and oxidation, so shielding gas or inert atmosphere must be used in the spraying process. The most common sprayed intermetallics are TiAl, Ti_3Al, Ni_3Al, and $MoSi_2$.

Polymers: growing number of thermoplastic, thermosetting polymers and copolymers can be thermal sprayed successfully including urethanes, ethylene vinyl alcohols (EVAs), nylon 11, polytetrafluoroethylene (PTFE), polymethylmethacrylate (PMMA), polyetheretherketone (PEEK), ethylene tetrafluoroethylene (ETFE), polyimide, polycarbonate, and copolymers such as polyimide/polyamide, polyvinylidene fluoride (PVDF) and Surlyn (DuPont). The most widely used thermal spray techniques for deposition of polymers are conventional flame spray and the HVOF. Their application areas include low-friction applications, chemical resistance and sealing.

- **Composite and Cermet Materials**

Metal matrix composite (MMC) material is a mixture of metal as a matrix with less than 80% of ceramic or another metal. The aim of MMCs fabrication is to have the optimal properties of both ceramic (e.g. hardness and wear resistance) and metal (e.g. ability to undergo plastic deformation). Cobalt, nickel, and molybdenum are the most common metals used as a matrix in MMC. MMCs are utilized as binder coatings in thermal barrier systems in order to compensate a thermal mismatch between substrate and top coating. Particulate-reinforced wear-resistant cermet coatings such as WC/Co, Cr_3C_2/NiCr, and TiC/NiCr are examples of the most common thermal sprayed composites.

- **Functionally Gradient Materials (FGM)**

Application of FGM materials are a growing approach to improve a performance of systems that subjected to the large thermal gradient, combine of corrosion and strength or wear resistance by means of cladding materials, and to improve electronic material structures for batteries, fuel cells, as well as thermoelectric energy conversion devices. The most typical application of FGMs is in the thermal barrier coatings (TBCs) in turbine components, rocket

nozzles, incinerator burner nozzles, chemical reactor tubes, and other critical furnace components

Chapter 3

Material and Experiment Producers

This chapter describes the coating materials, deposition technique, characterization and optimization of the coating, theoretical background of the corrosion and wear tests as well as experimental procedures.

3.1 Materials

The 1.0038 (S235JR) construction steel, which is a typical material for cylinder of paper machines, was used as a substrate with dimension of 40 × 50 × 8 mm^3. Prior to the coating process, all substrates were roughened in order to improve mechanical bonding of coating and substrate, using an injector blasting system at pressure of P=6bars and grit size of F16 and subsequently degreased with ethanol. Selected feedstock material was FeCrB powder alloy with two different powder fractions; -32+11µm and -20+3µm (GTV Verschleißschutz GmbH, Luckenbach, Germany). The chemical composition of the feedstock material is independent of the powder fraction and is given in Table2.

Table 2: Chemical composition of the feedstock and reference materials [wt.-%]

Materials	Fe	Cr	B	Ti	C	Si	Mn
FeCrB	Bal.	22.0-26.0	4.3-5.0	<0.3	0.4-0.7	-	-
FeCrBSiMnC	Bal.	27.5-29	3.8	-	0.1	1.5	1.5

Quite high Cr content was chosen to ensure a good corrosion resistance of the coating. Moreover, B promotes hard phases formation during spray process, which increases wear resistance. Also, presence of a few amount of Ti which reacts with C, allows more free Cr to form passive layer [84, 85]. As observe in Fig.8, the feedstock powder morphology is mostly spherical. It has been proved experimentally that spherical morphology supports

excellent flowability and reproducible powder feed rate up to high values. To minimize agglomeration effects, the powder was heated up to 120°C in a furnace before using it in the feeder system. A FeCrBSiMnC coating which applied by WAS, was chosen as reference coating system. As for the feedstock material of reference coating, the commercially available cored wires SP112 (Corodur Fülldraht GmbH, Willich, Germany) were used. The chemical composition of the wires is given in Table2 as well.

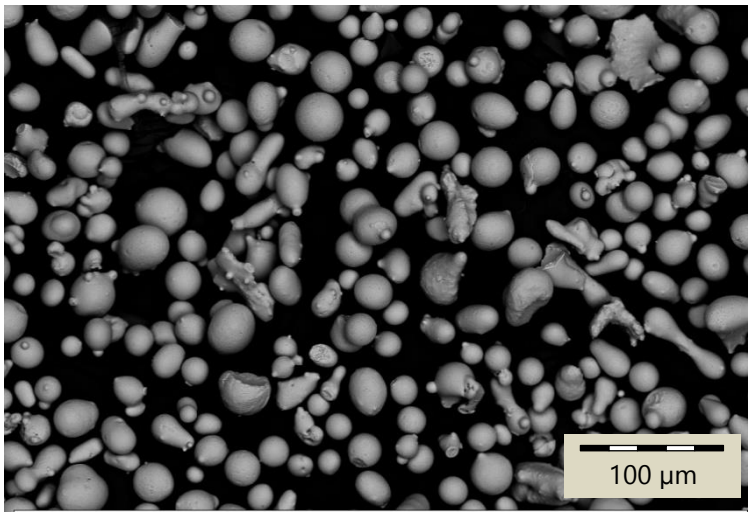

Figure 8: SEM-micrograph of the FeCrB powder alloy

3.2 Coating Deposition

The HVAF coatings were produced using an AK-07 system (Kermetico Inc., Benicia, USA) with presented experimental setup in Fig.9. The substrates were fixed into the sample holder. In order to rotatory movement of specimens, the sample holder was mounted onto an electromotor. The HVAF gun only moves into z-direction to coat the samples. The samples were cooled from two sides to reduce an accumulation of residual stress.

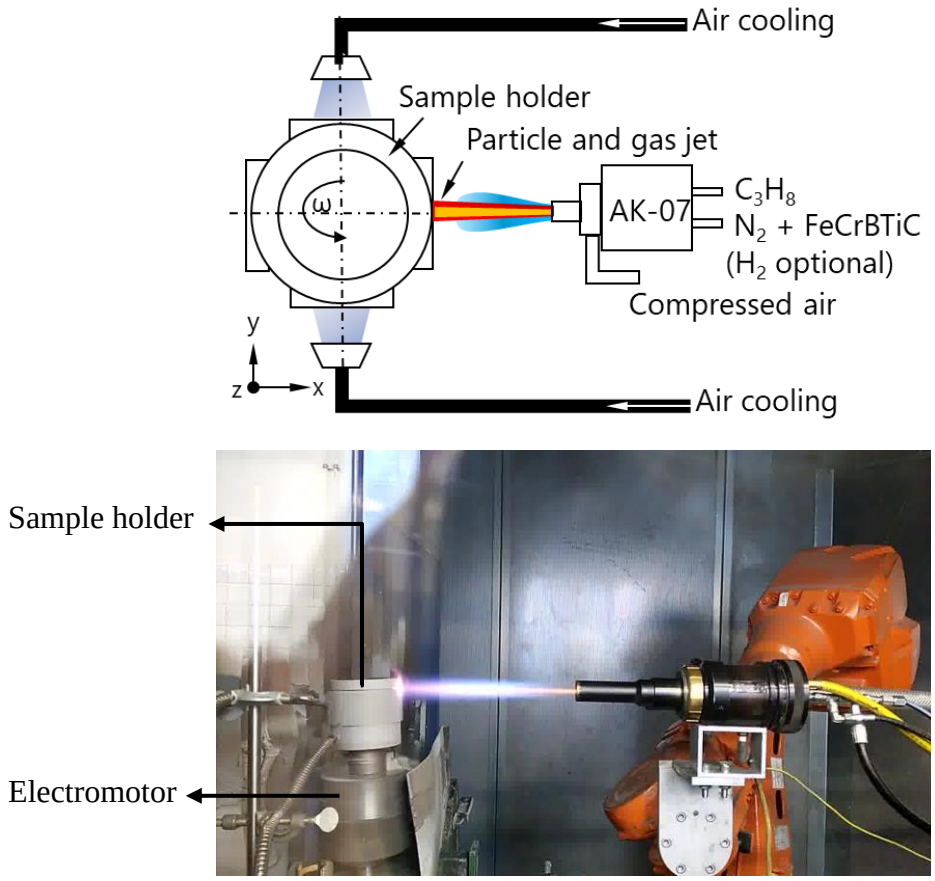

Figure 9: Experimental setup of the HVAF system

A number of spray parameter sets were initially employed and tested to reach the crack free coatings. In terms of coating quality, optimization of these parameters is essential. Final coating parameters for the HVAF coatings are given in Table3.

Table 3: Spraying parameters for the HVAF process

Parameter	**Value**
Gun	AK-07
Compressed air [bar]	6.3
Propane [bar]	5.6
Nitrogen [SLPM]	18
Hydrogen [SLPM]	35
Stand-off-distance [mm]	250, 180
Surface speed [mm/s]	900, 4500
Powder Feed rate, ṁ [g/min]	40, 200
Cooling air [bar]	1.5

Among the parameters, stand-off-distance (SoD) and surface speed had a great influence on crack formation in sprayed coatings. The SoD distance between the nozzle and the substrate is critical because the optimal particle temperature and velocity occur in one plane along the length of the spray stream. The surface speed is a speed of spray stream across the surface of substrate which can control the deposition rate in terms of unit thickness per pass buildup [44, 86]. For the power feed rate of ṁ=200 g/min the surface speed was increased to achieve higher amount of heat energy of flame per particle [87]. Also, for the finer powder fraction (-20+3µm) the SoD was reduced to increase velocity of in-flight particles which results greater compressive residual stress in the coating [88]. The different thicknesses of the coatings can be achieved by adjusting the number of transitions. In this project, coatings with two different thicknesses of 250µm and 140µm were produced. For the thick coatings, short break (10min) was applied during the spray process to reduce the local heat loads. Overall, eight series of coatings were deposited which are listed in the Table4.

Table 4: List of different coated samples

Sample name	**Powder fraction, D (µm)**	**Powder feed rate, ṁ (g/min)**	**Average thickness, S_{ct} (µm)**
D-32; ṁ40; thick	-32+11	40	250
D-32; ṁ40; thin	-32+11	40	140
D-32; ṁ200; thick	-32+11	200	250
D-32; ṁ200; thin	-32+11	200	140
D-20; ṁ40; thick	-20+3	40	250
D-20; ṁ40; thin	-20+3	40	140
D-20; ṁ200; thick	-20+3	200	250
D-20; ṁ200, thin	-20+3	200	140

Industrially established process parameters were used to produce the FeCrBSiMnC coatings with the WAS technique (G30/4SF-PushLD/U2, Oerlikon Metco AG, Winterthur, Switzerland) as a reference coating. The process parameters are shown in Table5. The WAS coating was produced with wire feed rate of ṁ=110g/min and thickness of 720µm. To increase corrosion resistance of reference coating, it was sealed with epoxy with industrial stablished sealer #HM2407 (Diamond Metallplastic GmbH, Moenchengladbach, Germany).

Table 5: Spraying parameters for the WAS process

Parameter	Value
Current [A]	150
Voltage [V]	30
Pressure [bar]	3.5
Stand-off-distance [mm]	150
Surface speed [mm/s]	600
Wire feed rate [g/min]	115

3.3 Coating Characterization

The HVAF-sprayed and the reference coatings were characterized to investigate their microstructure, phase composition, microhardness, topography and fracture toughness. Each investigation and its method is described in the following part.

3.3.1 Sample preparation

Metallographic preparation is a prerequisite step to characterize coatings. Inappropriate metallographic method may cause scratches, deformation, smearing, edge rounding, pullout, cracks, contamination, embedded abrasive, lapping tracks and staining. Therefore, it is vital to ensure that the proper grinding and polishing procedure is chosen. Metallographic preparation includes cutting, mounting, grinding, polishing and finally etching (described in appendix I). However there are some materials which do not need etching such as nitrides, certain carbides and intermetallic phases[89].

3.3.2 Microstructural analysis

The microstructure will strongly influence the coating properties. In other word, corrosion and wear behavior are affected directly by the microstructure of coating. In this regard, high amount of porosity will be detrimental to corrosion resistance because of higher penetration

of corrosive solution to the substrate. Furthermore, in terms of wear resistance it is essential to have uniform hard phases distribution as well as good cohesion between splats to prevent excessive wear damages. These characteristics as well as coating thickness can be investigated by a microscopical analysis of the coating's cross section. A light microscope is a simple method to observe a coatings structures as well as thickness measurement. A beam of light is directed to the observed surface and reflection of light provides a clear view of material surface. This type of microscope uses a magnification in the order 50-1000x and able to give quick results of the characteristics. To do so, the observed surface should be polished and grinded in order to have a mirror like surface with an adequate light reflection. In this study, cross section images were taken with a Zeiss Axiophot light microscope (Carl Zeiss AG, Oberkochen, Germany) to investigate and compare the microstructure of the HVAF and the WAS samples. Another way of characterization is a Scanning Electron Microscope (SEM), which is more complex and its resolution is close to the bonding distance of atoms. Two modes on the SEM can be used during the characterization; secondary electron mode and backscatter electron mode. First mode is useful to observe details in the surface, and backscatter mode lights up the elements compared to their atomic weight, which leads to distinguish the different phases of the coating. SEM has a superior resolution and depth of focus and provides more detailed and clear observations of the samples [90]. Thus, in this study, in order to have a higher magnification pictures from microstructures, the cross sections were also analyzed using SEM microscope (JSM 7000F1, JEOL Ltd., Japan) equipped with an energy-dispersive X-ray (EDX) microanalysis system. Line scan elemental analyses was also performed on the coatings cross section by electron probe microanalysis (EPMA, JEOL, JXA8530F, Japan).

3.3.3 Topography

The roughness of surface is a measurement of surface texture. Roughness is a crucial factor to understand how the surface and environment interact together. Since the dominant bonding mechanism of coating to the substrate in the HVAF technique is mechanical bonding, knowing the roughness of surface would be helpful to improve this adhesion. There are variety of ways to characterize the roughness of surfaces. The most common method in the industry is measuring of the Ra value (equation1). Ra is the average distance between the actual surface and central line of profile (Fig.10) [91].

Equation 1: $Ra = \frac{1}{L}\int_0^L |Z(x)|dx$,

in which L is the length measured and Z(x) is the peak value on point x compared to the set center line.

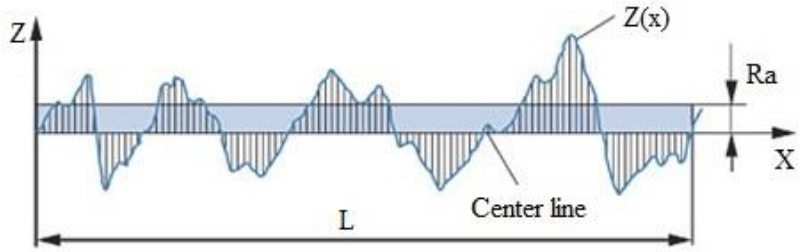

Figure 10: Schematic of surface roughness, Ra

It is expected that higher substrate roughness may be beneficial for particle/substrate bond formation due to the existence of a larger specific surface for adhesion of particles. In this project, surface roughness of the coatings in the as-sprayed state was measured with the confocal laser scanning microscope (CLSM) VKX 200 of Keyence Corporation (Osaka, Japan) (Fig.50 appendix ΙΙ). The CLSM that is a non-contact measuring instrument uses laser as the light source to measure the asperity of the target's surface. For a short description, first, the laser beam scans the surface of target. Then, the reflected beam pass through the half mirror and enters the light receiving element. At this point, the laser intensity of the received reflection, as well as the height position of the lens, are recorded by the microscope (Fig.11).

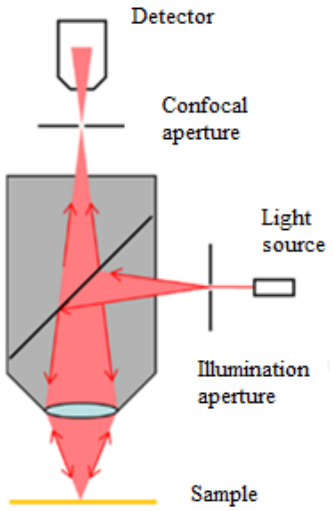

Figure 11: Principle of the confocal laser microscope [92]

3.3.4 Phase composition analysis

The X-ray diffraction technique is a characterization technique to identify structural properties such as strain state, phase composition, grain size, orientation, etc. The crystals of polycrystalline materials are made up of identical atomic planes. These planes have a uniform interplaner spacing d (Fig.12). When X-ray beam incidents to these family planes will be diffracted at certain angles known as a Braggs angle. Diffraction angle can be defined by Bragg's law [93]:

Equation 2: $n\lambda = 2d\sin\theta$,

in which n is an integer number; d is a lattice spacing of crystal planes (mm); θ is an angle of incident and diffraction (°) and λ is a wavelength of X-ray beam (mm).

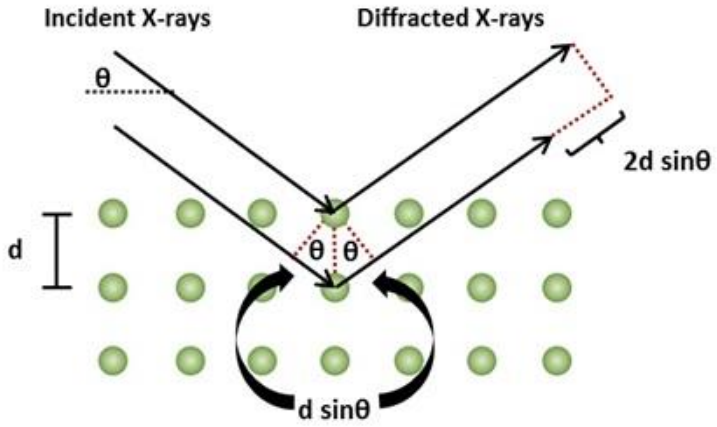

Figure 12: Schematic representation of the Bragg equation [94]

The XRD-spectra of all the HVAF coatings as well as feed stock materials were measured using Seifert XRD 3000 system of GE Sensing & Inspection (Technologies GmbH, Hürth, Germany) with a Cu-anode, Kα-radiation. The angle of incidence ω=10°, step width Δ2Θ=0.05°, holding time t_h=10s and measurement interval 2θ=20° to 80° were kept constant for all measurements. The obtained diffractogram was analyzed by a software program that can identify the different phases which were present in the coatings by comparison with the database of the program. By interpretation of results, it is possible to know the effect of spray process on chemical phases of coating materials. Moreover, identification of chemical phases can be useful to analysis the wear and the coorosion behavior of coatings.

3.3.5 Microhardness

The hardness properties have a significant influence on the wear resistance of materials. It is assumed that both adhesive and abrasive wear will often decrease as the hardness increases. However, the hardness is not the only wear affecting parameter, many other factors associated to wear such toughness and friction coefficient. There are three main methods to determine the hardness of materials; static indentation test, dynamic hardness test and scratch test. The static indentation tests (which carried out in the current research) are the most common method in which a ball, a diamond cone, or a pyramid is forced into the material. Typical hardness measurement methods are Rockwell, Brinell, Vickers and Knoop hardness test. The hardness measurement methods can be classified into macro- and microhardness measurement. The Rockwell and Brinell are the examples of macrohardness test. Microhardness test includes the Knoop and Vickers method. In Vickers hardness test the applied load is m=200g or greater, whereas the Knoop test is carried out at lower loads; less than m=200g [95] . In the current project, the Vickers hardness test was used to measure the microhardness values. As it sketched in Fig.13, Vickers hardness test utilizes a highly polished, pointed, square-based pyramidal diamond indenter with face angles of 136°, which is pressed against the material with a known force to make a squared shape mark. After that, the diagonals of indent are measured [95].

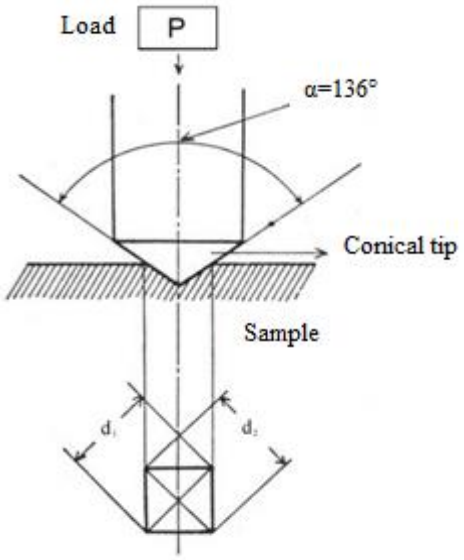

Figure 13: Schematic of the Vickers hardness test

The Vickers hardness number (HV) is the ratio of the applied load to the surface area of the indentation:

Equation 3: $HV=\frac{F}{A}\approx\frac{1.8544\times F}{d^2}$,

in which F is an applied force [kg] and d is an average diagonal of the indentation [mm].

The hardness test was done on the cross-section of the coatings. It is important to make sure that the indent area does not exceed from coating to the substrate, because the substrate is more soft compared to the coating and causes high deviation in the results. To measure the microhardness of coatings the cross-sections were prepared and polished to Ra < 0.5 μm. The microhardness of the coatings was measured with Micromet 1 (Buehler, Illinois, USA) (Fig.51 in appendix Π). For this purpose, the coatings were loaded with a weight of m=1000g. The hardness of each sample was measured 10 times to achieve statistically relevant data.

3.3.6 Fracture toughness

Fracture toughness is a mechanical property to quantitative express of material's resistance against brittle fracture when a crack is present. Measurement of fracture toughness for bulk materials is classical, and can be defined routinely using Charpy test, four-point or three-point bending, etc. [96]. However, these methods cannot be applied for coatings because of the size limitation of the coating thickness. Various methodologies have been developed for fracture toughness measurement of freestanding coatings. One approach for hard coatings bonded to substrates is a use of nano-indentation on coatings [97]. In this study, equation4 was used to measure the fracture toughness K_{1C} of thick coatings. This equation is only valid for a 'Half-Penny' crack regime that requires both a median and a radial crack pattern (see Fig.14 for definition of median and radial [98]). To ensure the complete formation of a half-penny cracking pattern, geometrically, it is required $\frac{c}{a} > 2.8$, where "a" is the Vickers half-diagonal (Fig.15). Also, equation4 typically is used for high applied loads [98, 99].

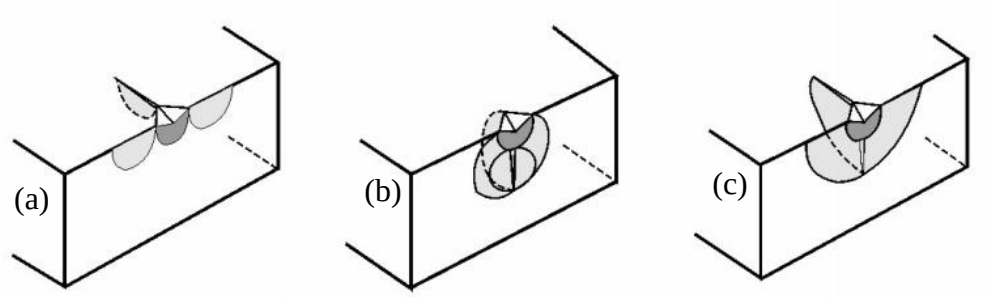

Figure 14: Crack patterns in a brittle material upon Vickers indentation: (a) a radial crack; (b) a median crack; (c) half-penny cracking (combination of a radial crack and a median crack)

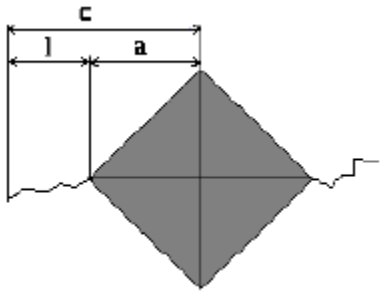

Figure 15: Schematic illustration of half-penny cracking regime for fracture toughness measurement

Equation 4: $K_{IC} = 0.0154 \left(\frac{E}{HV}\right)^{0.5} \left(\frac{L}{c^{1.5}}\right)$,

in which HV is a Vickers hardness; E is a modulus of elasticity; L is a crack length; C is a distance of crack tip to center of indentation.

The modulus of elasticity was determined by Fischerscope HM2000 XYp (Fig.51 in appendix П). In the Fischerscope, the Berkovich pyramid was used as an indenter and was pressed into the coating. The test load of F=1000mN was chosen. The load applied onto the sample increases continually until its maximum value was reached. After that, the load was kept constant for t=5s, then the test load was diminished. Throughout the entire load cycle, the indentation depth was measured. The geometry of the indenter and the shape of the mark left by the indenter in the material after the indentation process were taken under consideration in calculations of the mark's area. All measurements were conducted with n=10 repetitions for each coating to ensure statistical accuracy. The modulus of elasticity accomplished by means of plotting the values of the test load with respect to the indentation depth. As for the crack length, it can be determined during the microhardness measurement as well.

3.4 Aging investigation

The purpose of aging experiment is to simulate a real environment of Yankee cylinders in slightly aggressive medium and high temperature and then evaluation of coating behavior in terms of corrosion and wear properties. Therefore, the coated samples were put on top of the glass tubes which were filled with 0.5% NaCl-solution and were put in the furnace. The maximum temperature was set to 110 °C with holding time of 100 hours. Due to sealing of samples as well as the high temperature, samples were aged in saturated NaCl-steam atmosphere. After 50 hours, the tubes were taken out for visual investigation as well as pouring the electrolyte. The setup of aging experiment is shown in Fig.16.

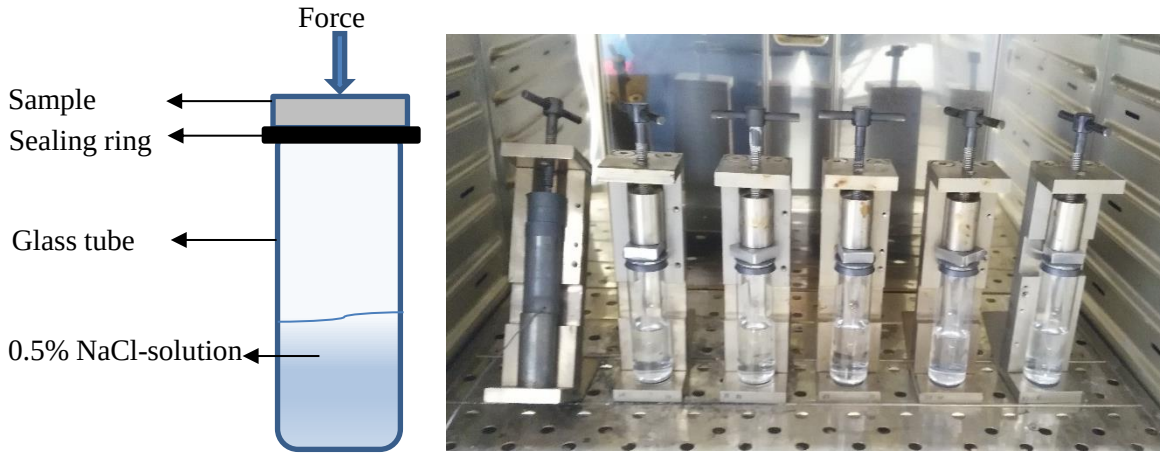

Figure 16: Aging test setup

3.5 Wear resistance against sliding

General term of wear is a process of removal of materials from one or both surfaces, which are in contact and have a relative motion. Although the rate of removal is usually slow, it is continuous and steady process [100]. To select a proper coating for wear resistance, understanding of the different wear mechanisms is necessary. There are some main categories of wear, which are based on quite distinct and independent phenomena.

3.5.1 Introduction of wear mechanisms

The wear mechanisms usually include abrasive, adhesive, tribochemical wear and surface spallation. In each mechanism, surfaces can have different relative movements such as rolling, sliding, fretting, impact, etc. In the following, abrasive and adhesive wear mechanisms, which are more dominant in the sprayed coatings, are described. The other wear mechanisms are explained in the appendix.

(1) Abrasive wear

The term abrasive wear is the wear mechanism that takes place when two surfaces have a relative sliding to each other. A two-body and three-body abrasive wear are the most widespread known abrasive wear modes. A two-body abrasive wear is scratch of softer surface with roughness peaks of hard surface. In three-body wear hard particles forced against and moving between two sliding surfaces [101]. Fig.17 illustrates these wear mechanisms.

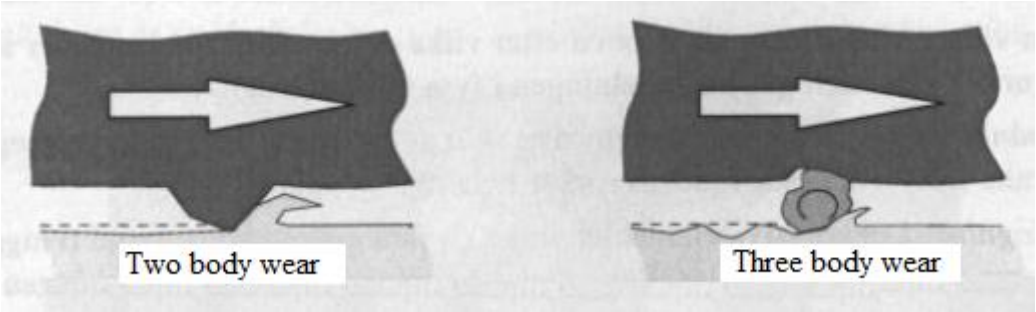

Figure 17: Abrasive wear modes [102]

(2) Adhesive wear

Adhesive wear [103] occurs in the same way as abrasive wear when two surfaces sliding relatively to each other, however, with a different mechanism. When two surfaces slide against each other with high force, the whole of the contact load is carried only by the very small area of asperity contacts; this may cause cold welding between surfaces (Fig.18). As a result, small local adhesion effect in the contact zone is produced. Sliding of surfaces will cause high shear force which leads to break of the adhesive junctions. As sliding continues, rupture will be formed. The probability of adhesive wear may be minimized by usage of lubricants.

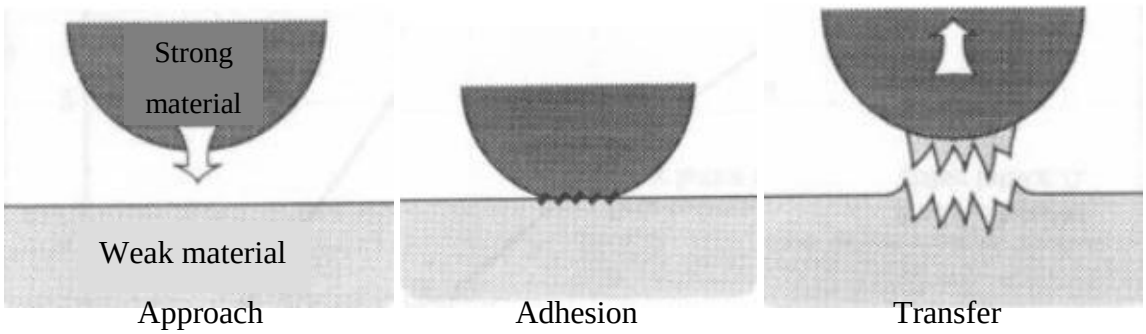

Figure 18: Adhesive wear mechanism

3.5.2 Pin-On-Disc test

The Pin-on-Disc wear test has been used widely to evaluate and investigate a friction and a wear resistance of dry and lubricated surfaces of bulk materials and coatings. The ASTM-G99 standard [104] indicates the laboratory procedure for determining the wear of materials during sliding using a pin-on-disk apparatus. A stationary pin or ball is pressed against a rotating disk of the material to be tested at a specified load usually by means of an arm or lever and attached weights (Fig.19). Wear rate can be determined by geometrical or mass loss methods. In the case of the mass loss method, the volume loss can be derived with dividing the mass loss by the density. In a geometrical method, by converting a measured linear dimension to a volume, using suitable mathematical relations, it is possible to achieve volume loss [104].

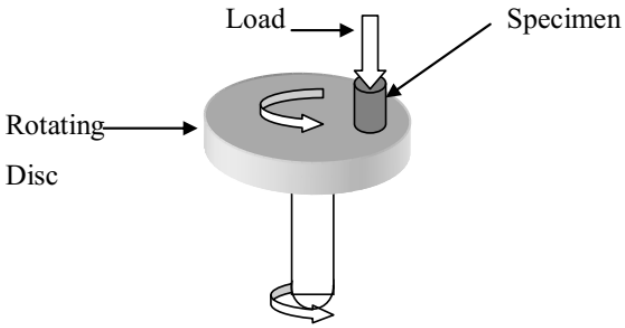

Figure 19: Diagram of Pin-on-Disk configuration wear test

For the investigation of the wear properties, a POD-tribometer of CSM Instruments SA (Freiburg, Germany) was used (Fig.54 in appendix Π). Prior to the wear tests, the HVAF and the reference coatings were cut to dimensions of 25×25×8 mm^3 and mechanically grinded and polished to the roughness of Ra < 0.5 µm to provide comparable initial conditions for all samples. An Al_2O_3 ball was used as a counter body to provide abrasive wear condition, reduce the adhesion effects as well as chemically inert environment. The test parameters are given in Table 6. The tests were performed without lubricant. Subsequent to the wear test, the wear tracks and a lost volume were investigated using CLSM (Fig.20.a). By multiplying the area of worn section (Fig.20.b) to the path's circumference ($\pi\ d_{pd}$), the lost volume V can be calculated. Finally, the wear coefficient K was determined with following formula:

Equation 5: $K[\frac{mm^3}{Nm}] = \frac{V}{F.(s.\frac{d_t}{d_{pd}})}$,

in which F is the normal load; d_{pd} is the path diameter; *S* is the wear track length and V is the wear volume.

Table 6: Pin-on-Disk test parameters

Parameter	Value
Path diameter d_{pd}	10 mm
Wear track length S	1000 m
Rotation speed	10 mm/s
Temperature	Room temperature
Normal load F	10 N
Counter body	Al_2O_3 , $ø_{cb}$=6mm

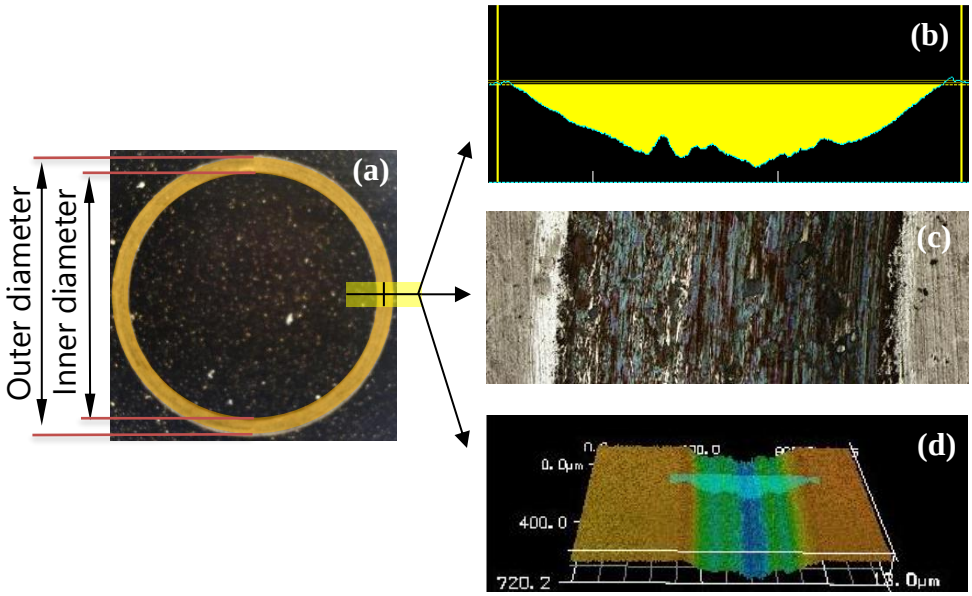

Figure 20: Determination of the wear volume V (a) Overview of whole wear track, (b) Cross-sectional area, (c) Section of wear track, (d) 3D picture of wear track section

3.5.3 Pin-On-Disc test of aged samples

In order to investigate effects of aging experiment on the wear behavior of coatings, the POD test was done also for aged samples in accordance with chapter 3.4.2. Subsequent to the wear test, the wear tracks and wear coefficient were compared to samples before aging.

3.6 Corrosion Test

3.6.1 Polarization test

Electrochemical corrosion tests are one of the main common techniques to evaluate the corrosion behavior of metals. In these tests, corrosion is an electrochemical process of oxidation and reduction reactions. When corrosion occurs, electrons are released by the metal (oxidation) and gained by elements (reduction) in the electrolyte. Due to the presence of electrons flow (current) in the corrosion reaction, it can be measured and controlled electronically. Therefore, controlled electrochemical experimental techniques can be utilized to characterize the corrosion properties of metals in various electrolyte solutions. Polarization test is one of these electrochemical techniques, which is able to measure and/or control the potential and current of the oxidation/reduction reactions. Polarization cell consists of an electrolyte solution, a counter electrode(s), a reference electrode and a working electrode which is an investigated sample. A triple-electrode cell is placed in the electrolyte solution and connected to an electronic instrument called a potentiostat (Fig.21). In the solution, an electrochemical potential (voltage) is generated between the electrodes. The corrosion potential (E_{corr}) is measured by the potentiostat as an energy difference between the working electrode and the reference electrode.

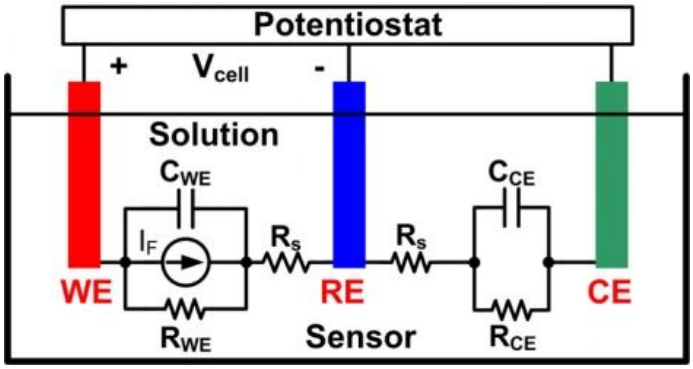

Figure 21: Schematic of polarization cell [105]

In the current project, the polarization test and subsequent cross-section analyses of the corroded samples were performed to determine corrosion resistance of coatings. The polarization test was carried out in a 5 % NaCl-solution with a pH-value of 7.0 ± 0.1 at room temperature using Reference 600^{+} of Gamry Instruments (Warminster, England) (Fig.53 in appendix Π). A Calomel (Hg_2Cl_2) electrode was used as reference electrode and the potential scan rate was set to 0.5 mV/s. Prior to the polarization test, specimens were cut with

dimension of 25×20×8 mm^3, and then prepared in the same manner as for the pin-on-disk test. The rest potentials and the corrosion current densities were investigated using the Tafel slope analysis according to Faraday's law. Afterward, cross sections were prepared to detect whether corrosion only occurred in the surface or also at the interface of coating and substrate.

Chapter 4

Results and Discussion

The results and discussion are categorized into coatings characterization, mechanical properties as well as corrosion test. Thus, the discussion of observations and findings are given in coming appropriate classified headings.

4.1 Coatings characterization

4.1.1 Microstructure

Fig.22,23 reveal the cross-sections of the as-sprayed HVAF coatings that were taken with light microscope. All coatings showed very dense microstructure, crack free, negligible oxide particles, with a barely visible particle boundaries, proving good inter-particle bonding. A little dark contours were detected occasionally at the interfaces between the partially molten particles in coating. Microstructures consist of low amount of porosity, which are mostly present in a near-surface region of all coatings. This has been reported as a characteristic of high-kinetic thermal sprayed HVAF coatings where the lack of particles hammering [38, 106] in the last deposited layers leads to produce porosity in near-surface layers. It is worth saying that in most practical cases, the outer porous layer is entirely removed by grinding and polishing before use. Porosity has been shown as a critical parameter that can significantly affect the corrosion behavior of thermal spray coatings [107, 108]. The pores allow the electrolyte to penetrate and attack the substrate chemically [109]. Another aspect of cross-sectional micrographs with a low magnification is a pretty good bonding between coating and substrate. Only some grit blast residues are present at the interface which have produced during preparation process.

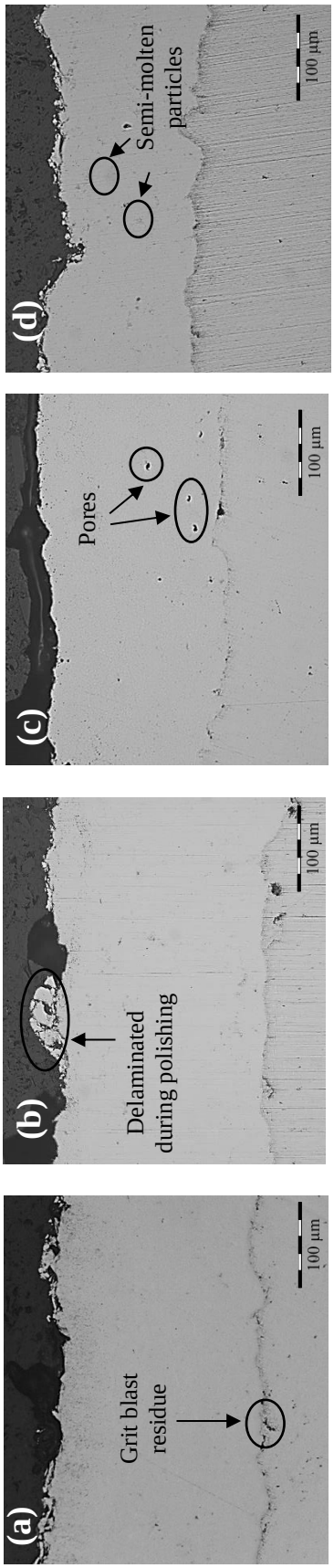

Figure 22: Cross-section of D-32+15µm as-sprayed coatings (a) ṁ200; thick, (b) ṁ40; thick, (c) ṁ40; thin, (d) ṁ200; thin

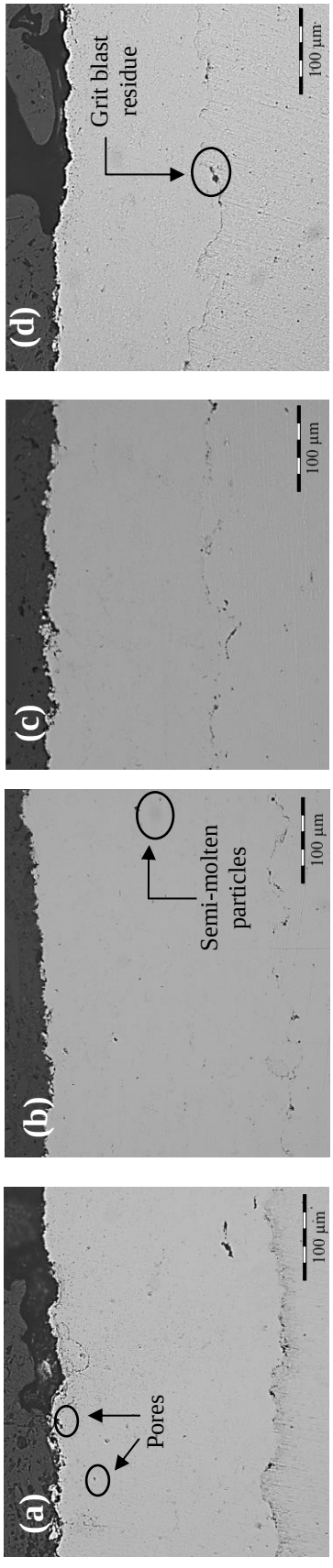

Figure 23: Cross-section of D-20+2µm as-sprayed coatings (a) ṁ200; thick, (b) ṁ40; thick, (c) ṁ40; thin, (d) ṁ200; thin

Detailed coating structures are presented in Fig.24 which analyzed by SEM using backscattered electrons (BSE). For both powder fraction coatings, two regions could be detected; dark gray area which surrounded with bright gray region [36, 110]. Based on the chemical composition, it is assumed that the dark gray phases present segregation as borides (Fe,Cr) and the surrounding bright gray phases are corresponded to Fe-based phases containing Cr and B. To verify the mentioned hypothesis the high magnification EPMA line scan is shown in Fig.25. It is also worth underlining that due to the different solidification rate, the shape of dark precipitates are not same in the fine and coarse powder. In the fine powder coatings, borides were cooled faster and had much more time for solidification, which leaded to spherical-shaped precipitates. On the contrary, coarse powder fraction coatings were subjected to slower cooling rate and produced long-shaped precipitates.

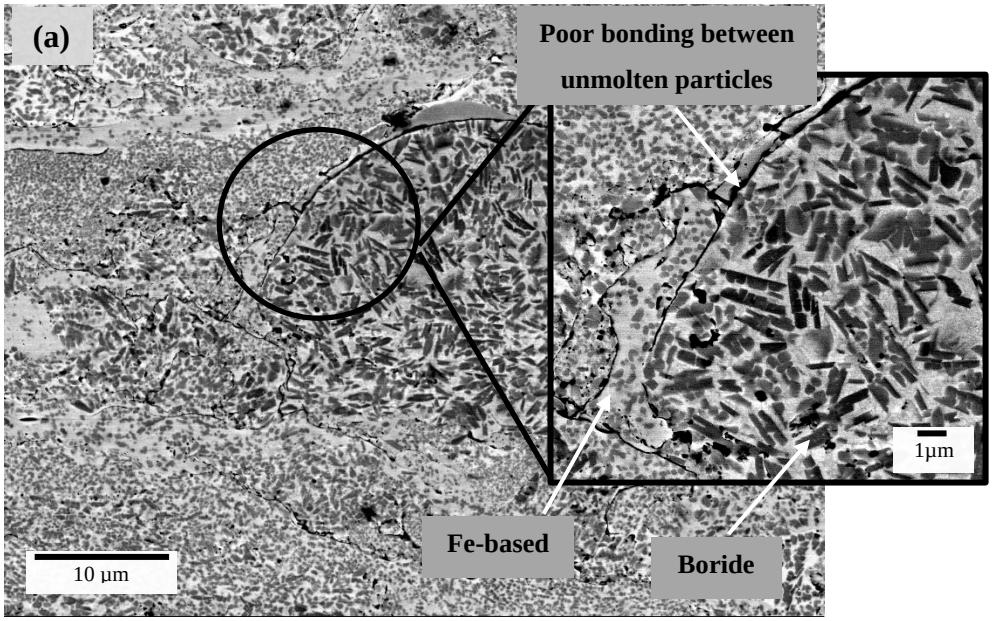

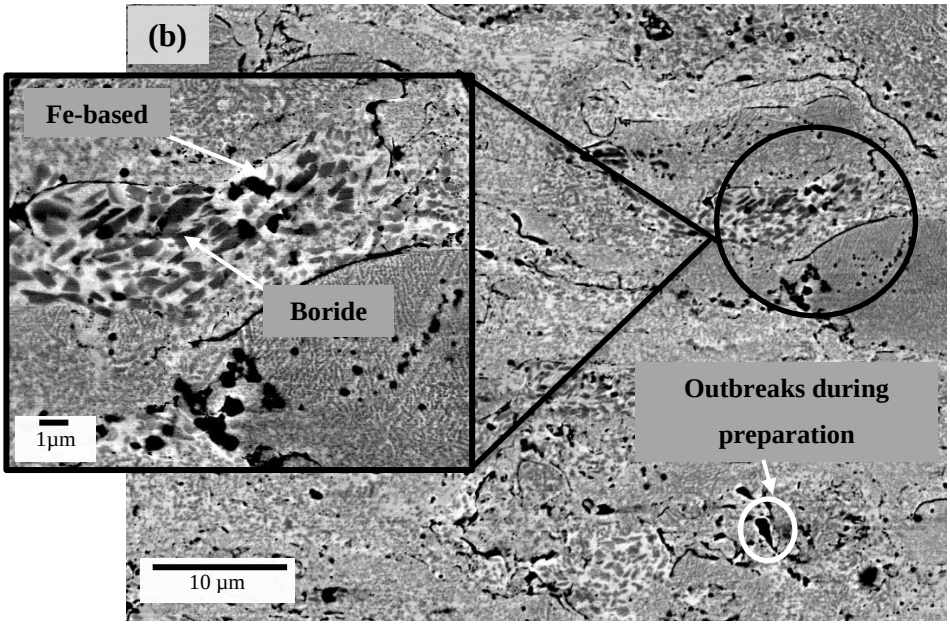

Figure 24: SEM image of HVAF sprayed coatings, (a) D-32; ṁ200 (b) D-20; ṁ200

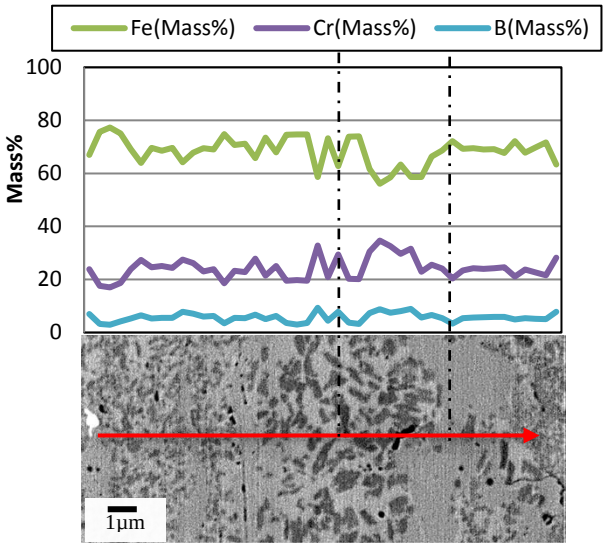

Figure 25: EMPA line scan microanalysis on the corresponding SEM investigated area of HVAF coatings

Fig.26 compares the SEM cross-sectional views of the WAS and the HVAF coatings. The WAS coating has a fairly porous structure with oxidized particles as well as more visible lamellar structure with elongated splats parallel to the substrate. Higher amount of oxide particles and porosity with respect to the HVAF-sprayed coating resulting inferior wear and corrosion properties, as it will be discussed in the next chapters.

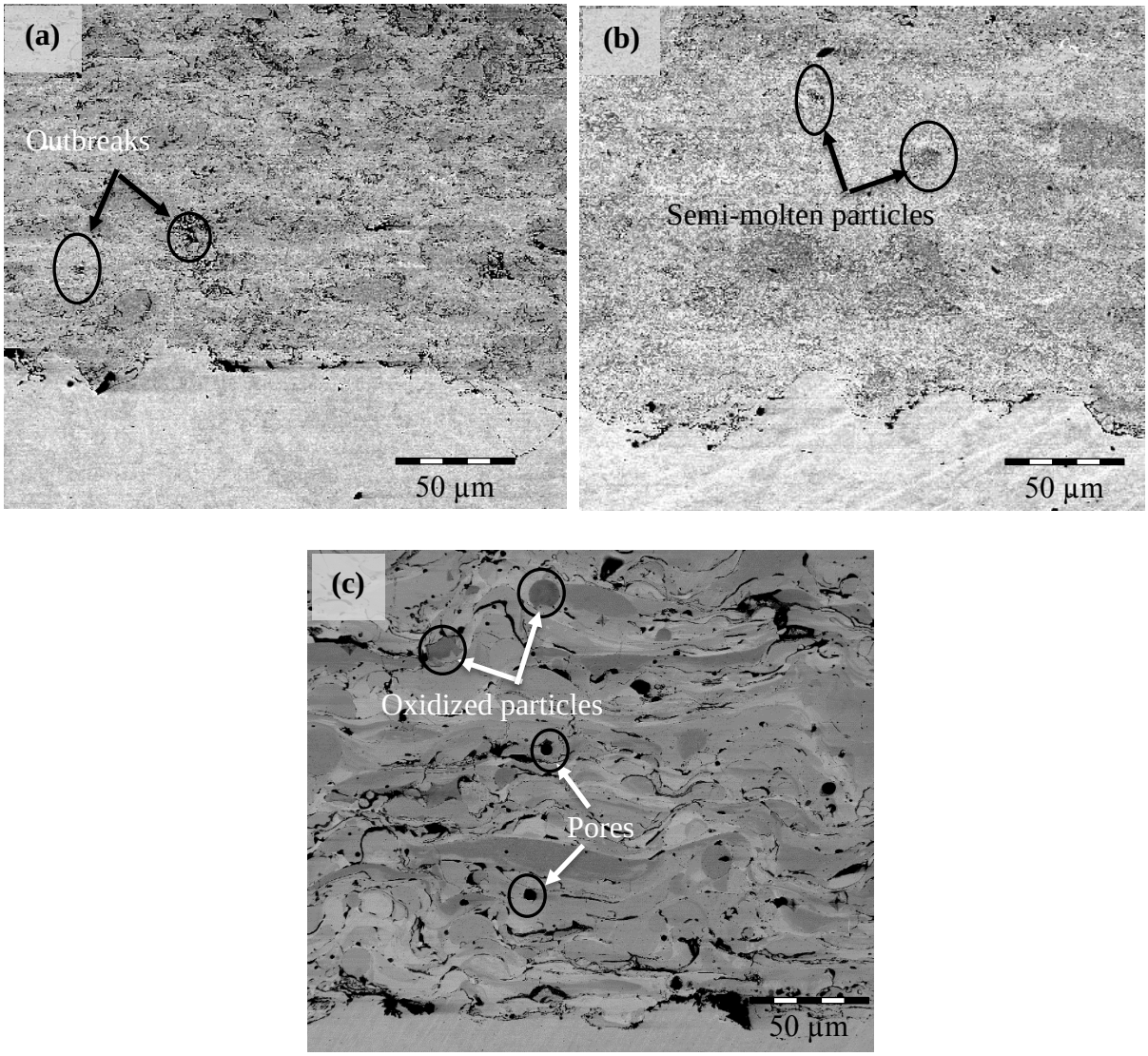

Figure 26: The SEM pictures (a) HVAF; D-20; ṁ200, (b) HVAF; D-32; ṁ200, (c) WAS; ṁ110

The as-sprayed roughness of the coatings are given in Table7 and Fig.27. Among the HVAF coatings, finer powder fraction (-20+3µm) produced more smooth surface compared to coarse powder coatings (-32+15µm). Moreover, roughness of the WAS reference coating is significantly higher that the HVAF coatings which resulted from lower particles velocity and plastic deformation [111]. Smoother surface causes a near net shape geometry and consequently less post production time as well as saving resources. Furthermore, the HVAF-sprayed coatings have a much lower thickness compared to the WAS even with higher powder feed rate. Thinner coatings can save feedstock material, decrease the production time and lead to energy saving due to the reduction of the thermal insulation effect.

Table 7: As-sprayed roughness of HVAF and reference coatings

Coating	Roughness R_a (µm)
D-32; ṁ40; S_{ct}:250	6.17±0.19
D-32; ṁ200; S_{ct}:250	5.91±0.49
D-32; ṁ200; S_{ct}:140	6.44±1.26
D-32; ṁ40; S_{ct}:140	5.46±0.39
D-20; ṁ200; S_{ct}:140	4.36±0.25
D-20; ṁ200; S_{ct}:250	4.08±0.19
D-20; ṁ40; S_{ct}:250	4.43±0.26
D-20; ṁ40; S_{ct}:140	3.90±0.24
WAS, ṁ110; S_{ct}:720	23.70±2.69

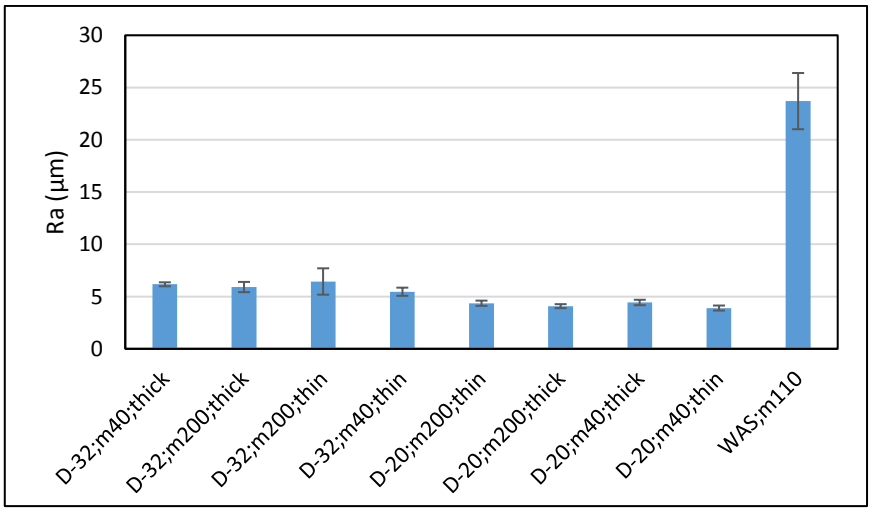

Figure 27: As-sprayed roughness of coatings

4.1.2 Phase composition

The XRD patterns of the Fe-based feedstock and the coatings sprayed by the HVAF are compared in Fig.28. According to the XRD patterns, detected phases were FeCrB and α-phase (Fe,Cr) and peaks were correspond to 43.2°, 44.7°, 50.41° and 56.3°. Moreover, both the coatings and the feedstock had a comparable pattern, which indicates there were no detectable changes in the phase analysis between the feedstock and the HVAF coatings. This specifies that not only there is no substantial oxidation of the materials during the HVAF spraying of feedstock powders, but also there is no generated residual stress by phase transitions. Another aspect of XRD patterns is that the sharp α-phase peaks in the feedstock material have become slightly broader and weaker in the coatings. This phenomenon can be due to two reasons. First, transition of ferrite to austenite during spraying process. Second, producing amorphous or partly amorphous coatings due to the rapid cooling of fully molten particles [87]. In order to better explanation, further analysis required such as BSE and EDX.

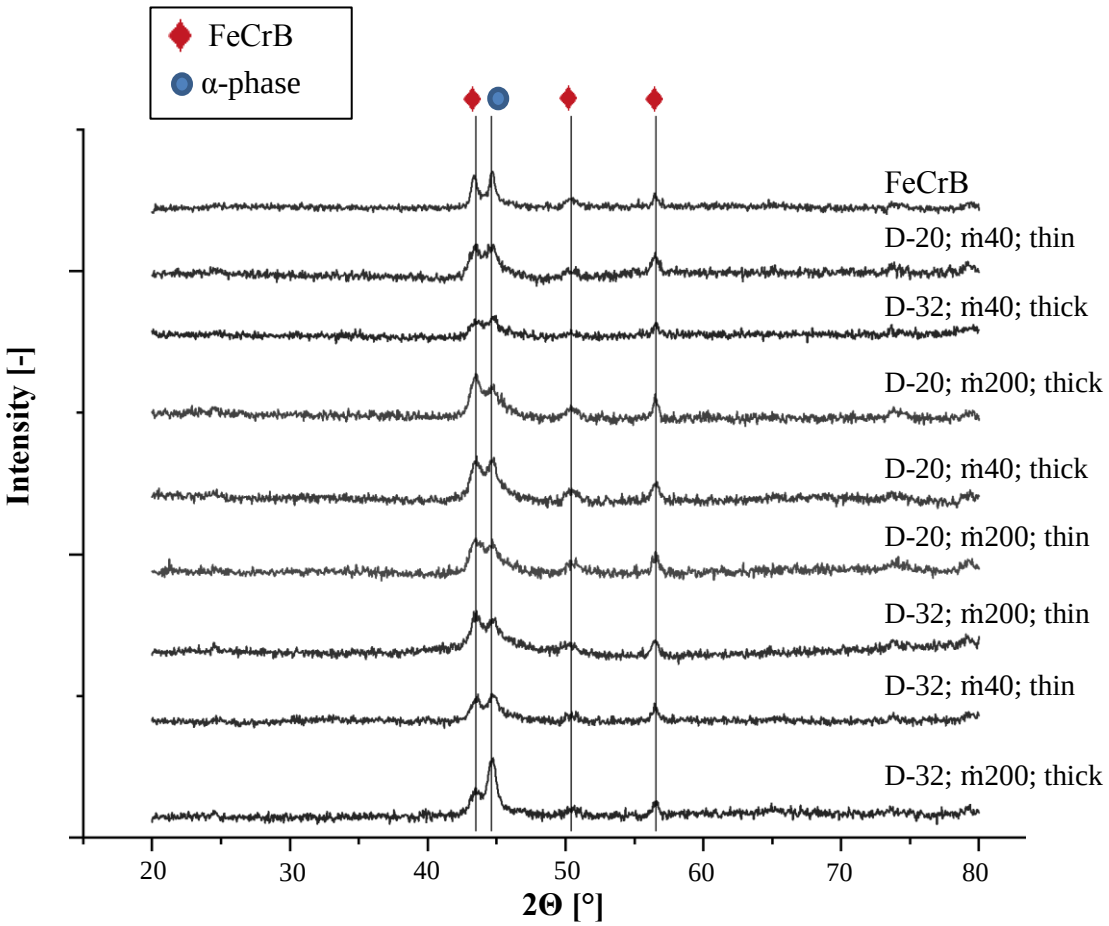

Figure 28: The XRD analyses of the HVAF samples and the feedstock material FeCrB

4.2 Mechanical properties

In the following part, the results of mechanical properties of the deposited coatings are presented include microhardness, fracture toughness, indentation modulus and wear behavior.

4.2.1 Microhardness

The results of the microhardness measurement for thick[8] HVAF coatings, reference coating and substrate are displayed graphically in Fig. 29. All the HVAF coatings have a much higher hardness than the substrate. The presence of borides (Fe or Cr) in the coatings is probably one reason for the higher hardness values. High hardness is a benefit for wear resistance because the hard borides could offset an external stress effectively. Among the HVAF coatings, those obtained from the ṁ=40g/min yielded much higher microhardness respect to the ṁ=200g/min coatings, because with the feed rate decreasing, the molten degree of spray particles increases, which resulted in the increase of hardness. The relatively low hardness of the WAS coating compared to the HVAF coatings can be due to the higher oxygen content in the WAS. Since, oxides locating at the boundaries between the partially molten particles usually have a loose structure, thus decrease the hardness. Moreover, It is well understood that an increase in amount of porosity decreases the coating hardness [112].

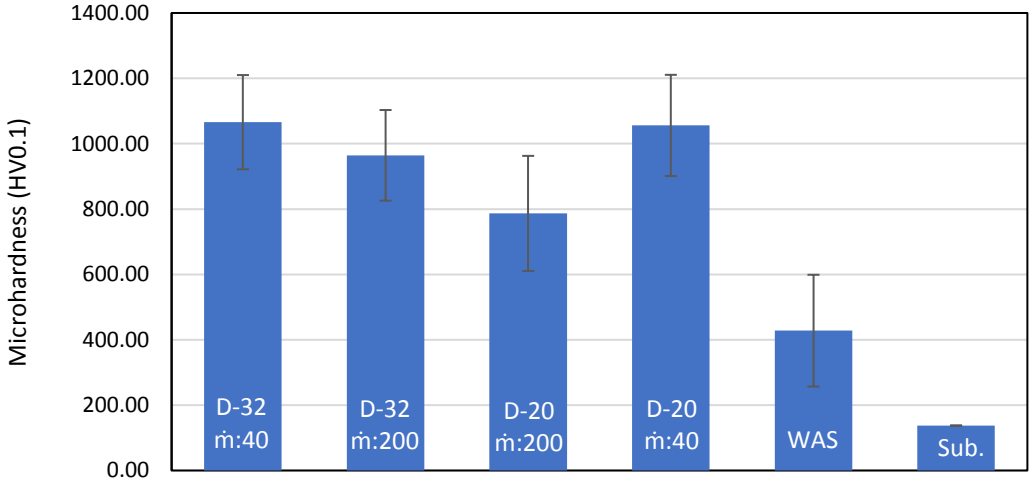

D-32; ṁ:40	D-32; ṁ:200	D-20; ṁ:200	D-20; ṁ:40	WAS	Substrate
1065,89±144	964,36±138	786,69±176	1055,95±154	428.4±171	137.25±1.06

Figure 29: Vickers microhardness of the HVAF and the reference coatings

[8] It was not possible to measure the hardness of thin coatings. Higher residual stress of thin coatings and high used force caused rapid growth of cracks during indentation.

It is worth saying that all the HVAF coatings have a high standard deviation with regard to their microhardness, which is typical for thermally sprayed coatings. It means the microhardness of the coatings varies, depending on the position of the indentation. In addition, Fig.30 presents the indentation marks during the measurement.

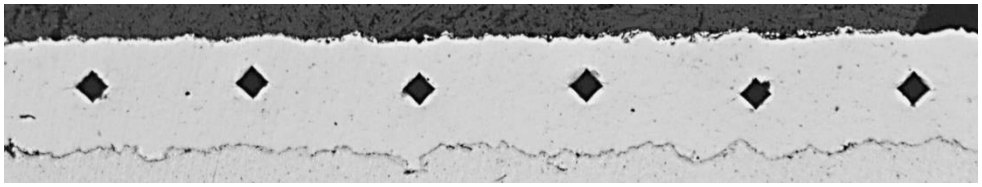

Figure 30: Indentation marks during modulus measurement

4.2.2 Fracture toughness

According to Fig.31, produced cracks during indentation test mainly propagate parallel to the coating/substrate interface direction, which corresponds to anisotropic crack propagation in the HVAF spray coating layers, and results from the elongated nature of the splats and the residual stress fields.

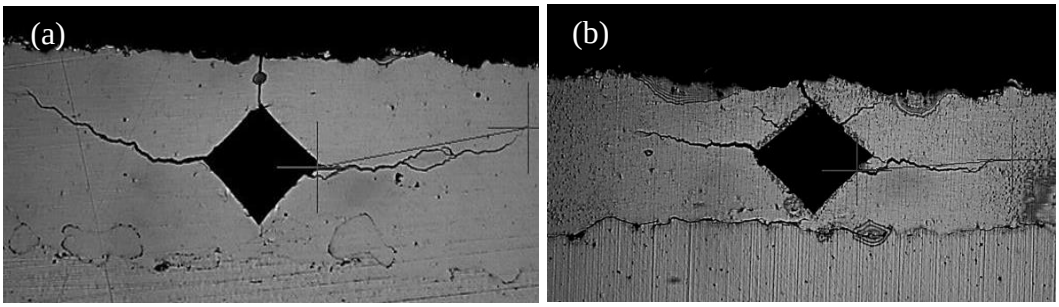

Figure 31: Micrographs of Vickers indentations (a) D-20, ṁ40; (b) D-32, ṁ200

Measured crack lengths, indentation modulus and fracture toughness of thick[9] coatings are summarized in Table8 and Fig.32. It is evident that the crack length decreased for the higher powder feed rate (200 g/min) due to lower melting degree which results in the higher compressive residual stress which not only resists against grow of cracks but also can close the cracks tip. For the same reason the fracture toughness of ṁ=200g/min coatings is higher with respect to the ṁ=40g/min. It was not possible to measure the crack length of reference coating because the cracks were very short and their energy absorbed with the porous structure and splats outbreaks (Fig.33). The average fracture toughness of HVAF sprayed

[9] Thin coatings did not have Half-Penny crack regime requirements (c/a ≥2.8)

coating is comparable and even higher than reported values for the HVOF sprayed Fe-based coatings [113] and ceramic coatings such as alumina [114, 115]. The high fracture toughness of sprayed HVAF coatings indicates that they have an ability of absorption of energy during deformation up to fracture. In other word, the coatings have a stress resistance to fracture in presence of a flaw. On the other hand, high fracture toughness is beneficial to wear resistance of coatings.

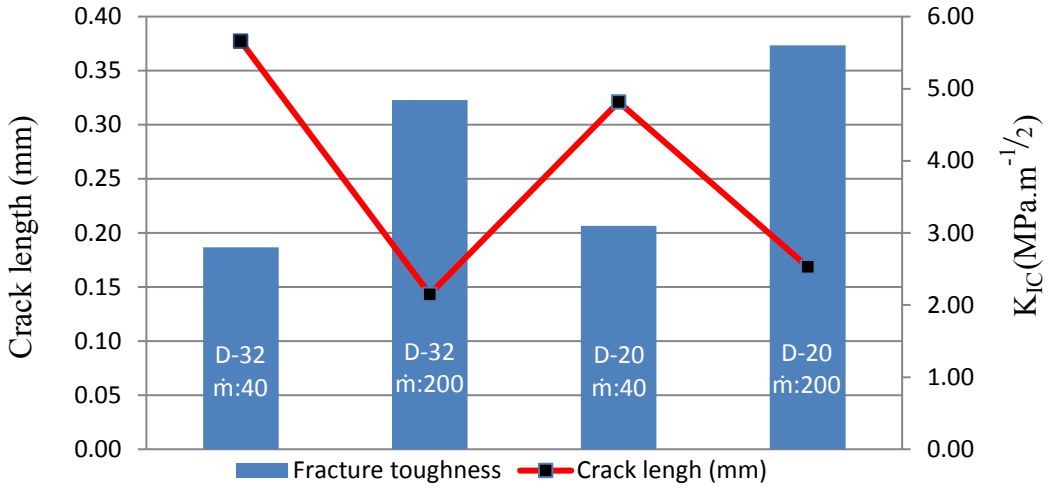

Figure 32: Crack length and fracture toughness of HVAF thick sprayed coatings

Table 8: Average values and standard deviations of indentation modulus, microhardness, crack length and fracture toughness for HVAF sprayed coatings

Sample	D-32, ṁ:40	D-32, ṁ:200	D-20, ṁ:40	D-20, ṁ:200
Crack length (mm)	0,38	0,14	0,32	0,17
Indentation modulus, E (GPa)	194,35±18.35	179,72±12.19	205,78±14.10	155,33±24.01
Fracture toughness, K_{IC} ($MPa.m^{-1/2}$)	2,80	4,84	3,10	5,60
Microhardness, HV	1065,89±144.19	964,36±138.78	1055,95±154.87	786,69±176.08

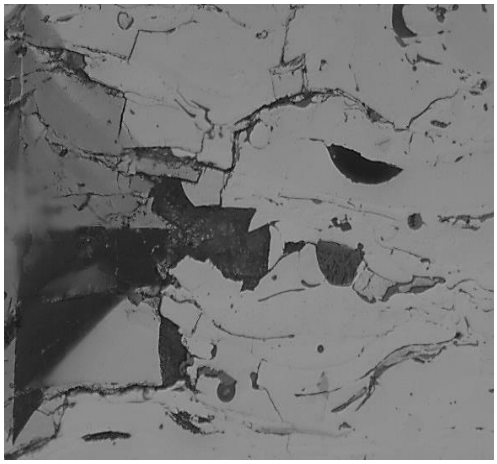

Figure 33: Indentation mark of the WAS coating and crack status

4.2.3 Wear measurements

4.2.3.1 Pin-On-Disk experiment

For the qualitative assessment of wear behavior of coatings, the wear tracks after POD test were investigated. Fig.34 compares the wear track of the substrate, the WAS and the HVAF coatings. The confocal microscopy images of the wear tracks claim that all samples have an abrasive wear condition and splats breakout. Moreover, the HVAF coatings are less prone to wear than the investigated WAS coating and the substrate due to the more homogenous wear as well as lower amount of coating breakout. Obviously, porous microstructure with a lower hardness promotes the breakout of splats. According to Fig.35, the height of wear track for substrate is ~420 µm. This value is decreased to ~170 µm and ~40 µm for the WAS and the HVAF coatings respectively, indicating that the wear resistance has significantly improved. This fact can be seen also in Fig.37 that the alumina counterpart of WAS coating was more worn respect to alumina of HVAF coatings. To confirm the mentioned qualitative assessment, the wear coefficient of coatings was measured and are shown in Fig.36.

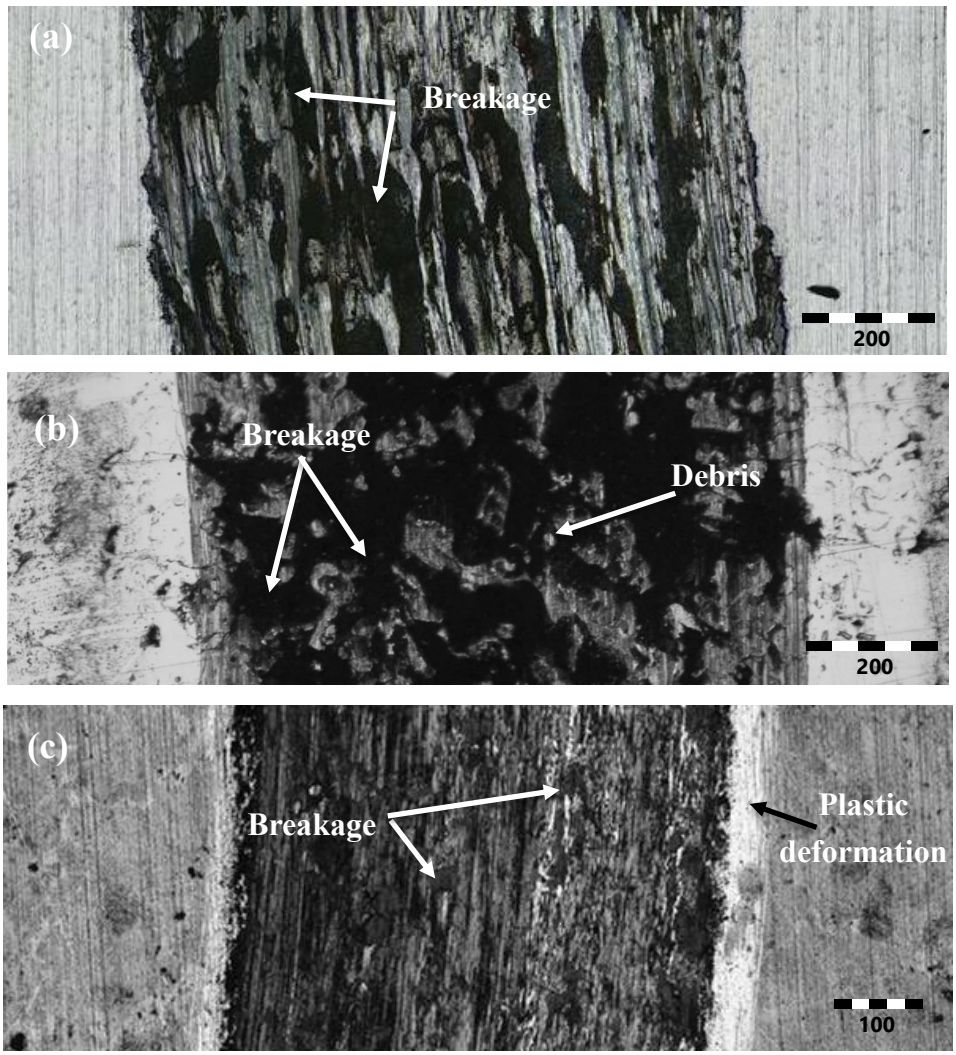

Figure 34: The confocal microscopy image of the wear tracks (a) substrate (b) sealed WAS (c) HVAF

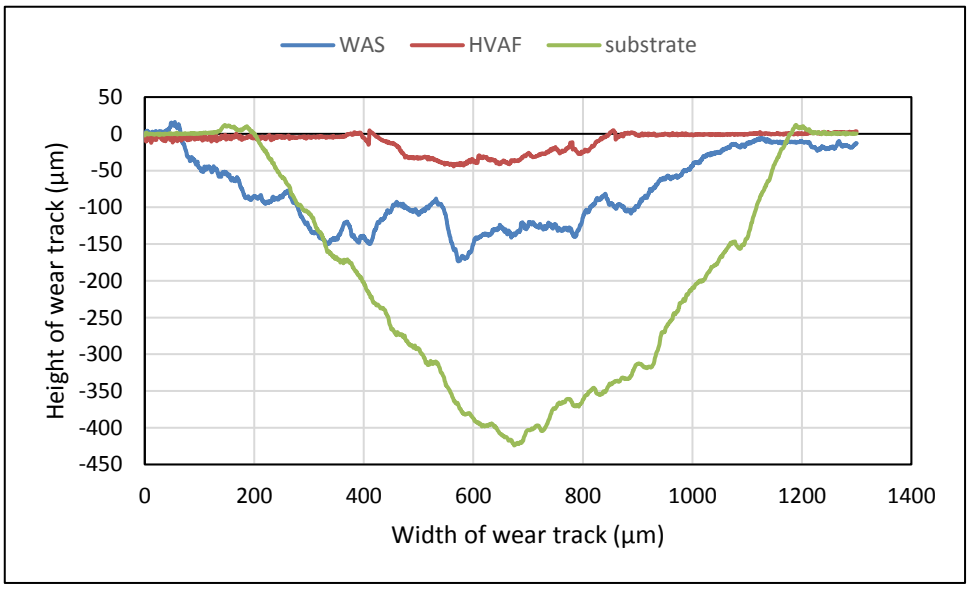

Figure 35: Height and width of wear tracks

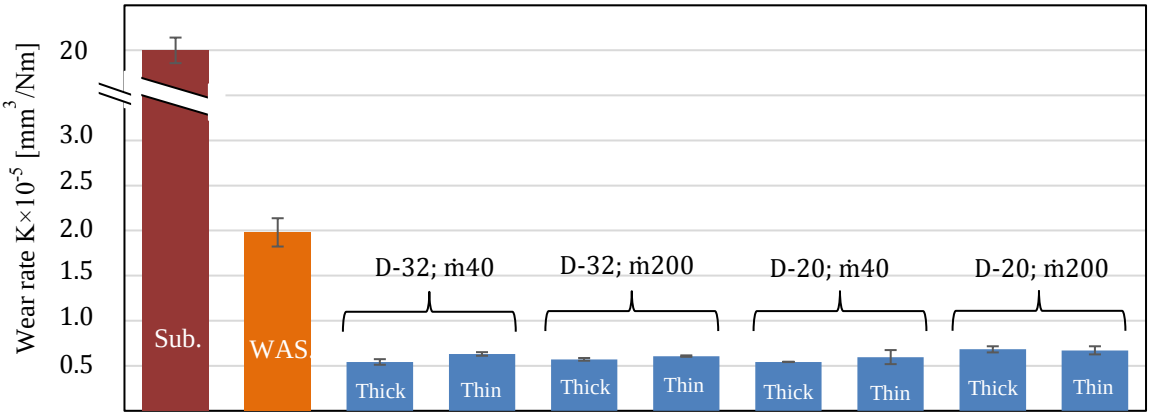

K [mm^3/Nm]	210.00	19.8	5.42	6.31	5.71	6.07	5.43	5.96	6.82	6.71
SDV [mm^3/Nm]	1.42	1.57	0.31	0.20	0.15	0.08	0.02	0.78	0.34	0.45

Figure 36: Wear coefficient K of all samples (All numerical values × 10^{-6})

Overall, the wear coefficient K of all the HVAF coatings is significantly lower with respect to the substrate and reference coating, which indicates better wear resistance of developed coatings with the chosen condition. The high K of the WAS coating refers to its porous microstructure which can negatively influence the wear resistance. The standard deviation of some HVAF samples are higher than others, which might be due to the larger outbreaks or debris at the surface of these coatings. Another aspect of wear coefficients is that for the HVAF coatings all K values are in the same range, which states neither powder feed rate nor powder fraction, have an influence on the wear behavior.

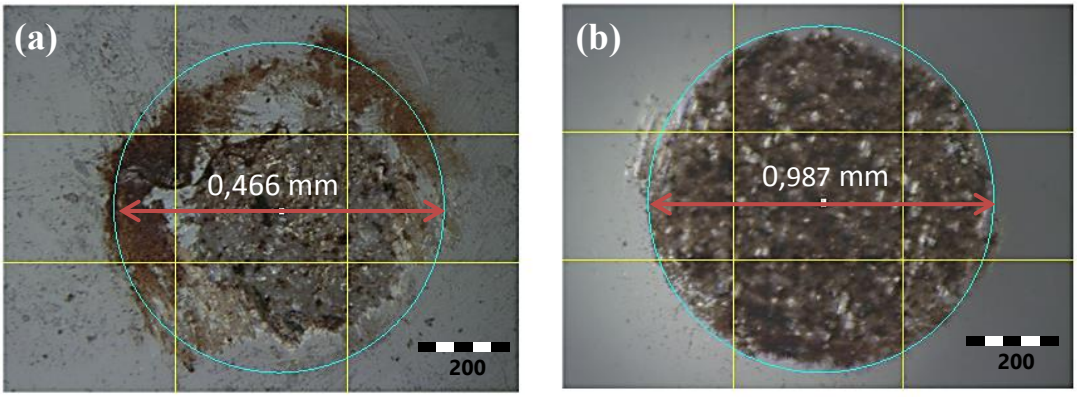

Figure 37: Optical micrographs of the wear mark on the alumina counterpart after ball-on-disk sliding wear testing against HVAF; D-20; ṁ:200 coating (a), WAS coating (b)

4.2.3.2 Pin-On-Disk of aged samples

In order to evaluate an effect of aging experiment on the wear behavior of coatings, wear coefficient of aged samples after POD test were determined. As it presented in Fig.38, the wear coefficient of the WAS coating before and after aging is noticeable higher compared to the HVAF coatings. Furthermore, K values for the HVAF coatings after and before the aging experiment were at the same range with slightly increase in some cases. Accordingly, it can be assumed that the aging test has not affected the cohesion of the HVAF coatings. On the contrary, the cohesion of the reference coating decreased due to formation of corrosion products. Fig.39 compares the 3D and cross-section pictures of wear track after aging test for one of the HVAF sprayed coatings and the WAS coating. The arrows indicate the abrasive grooves which produced during wear test with breakout splats of coating or debris.

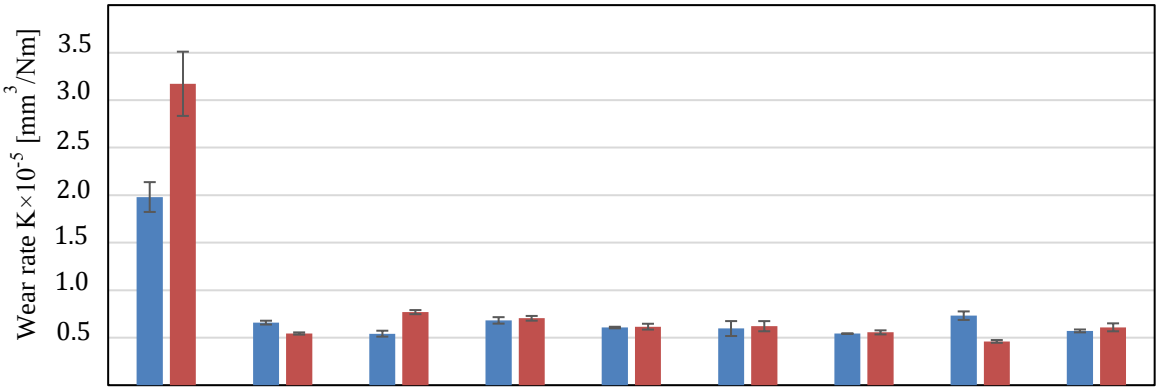

	WAS	D-32 ṁ:40 thin	D-32 ṁ:40 thick	D-32 ṁ:200 thin	D-32 ṁ:200 thick	D-20 ṁ:200 thick	D-20 ṁ:200 thin	D-20 ṁ:40 thick	D-20 ṁ:40 thin
Before aging	19,8	6.59	5,42	6.82	6,07	5,96	5.43	6,71	5.71
After aging	31,72	5.44	7,69	7.04	6,16	6,21	5.56	4,61	6.09

Figure 38: Comparison of wear coefficients before and after aging test for HVAF and reference coatings. All numerical values .10^{-6}

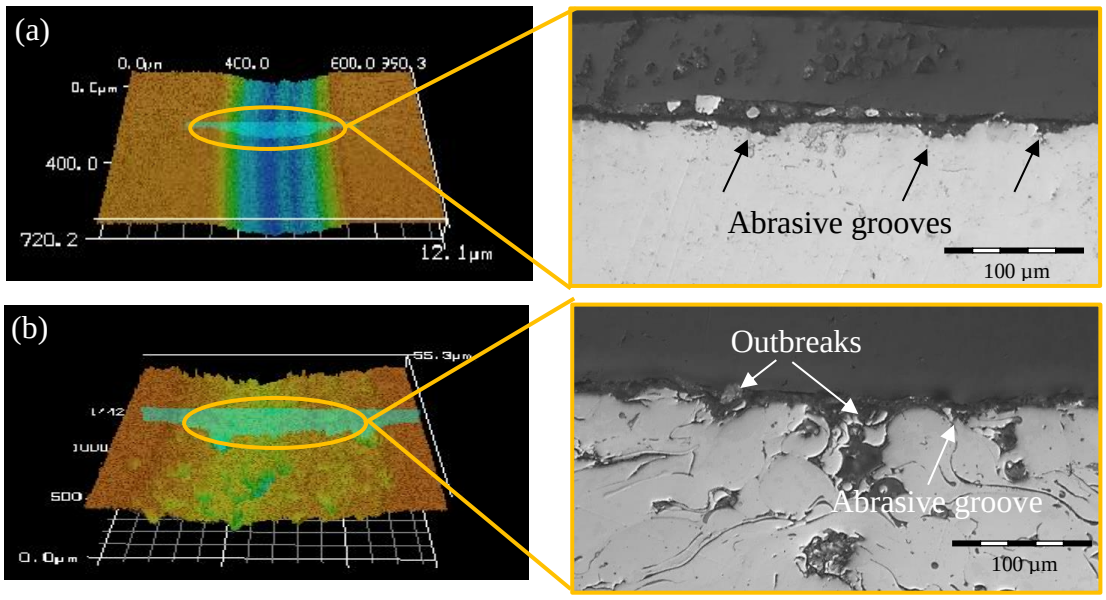

Figure 39: 3D and cross-section pictures of wear track: (a) HVAF; D-20; ṁ200, (b) WAS

4.3 Corrosion test

4.3.1 Polarization test

Tafel polarization plots of the fine and coarse powder fraction coatings prepared by the HVAF in comparison with the steel substrate and the WAS coating are presented in Fig.40,41 respectively to illustrate the overall kinetics of the corrosion process. Moreover, electrochemical parameters including the corrosion potential (E_{corr}) and corrosion current density (i_{corr}) are summarized in Table9. As shown the polarization curves of the HVAF coatings were shifted towards more noble values of rest potential and lower corrosion current density compared to that of the substrate and the reference WAS coating; providing better chemical resistance in chlorine environment. The thick and thin coating of HVAF;D-32;ṁ200 have a comparable rest potential with the WAS coating, indeed have a lower corrosion current density. Among the HVAF coatings, the noblest one is the HVAF;D-32;ṁ40 with the highest rest potential (-284.6 mV) and lowest current density (0.554 mA) which illustrates formation of stable and protective passive layer. In addition, it is evident from polarization curves that the HVAF coatings with a lower powder feed rate (ṁ40 g/min) exhibited lower current density. As the corrosion current density can directly be attributed to the corrosion rate, the higher powder feed rate coatings (ṁ200 g/min) would corroded rapidly with higher corrosion depth. (Fig.42,43)

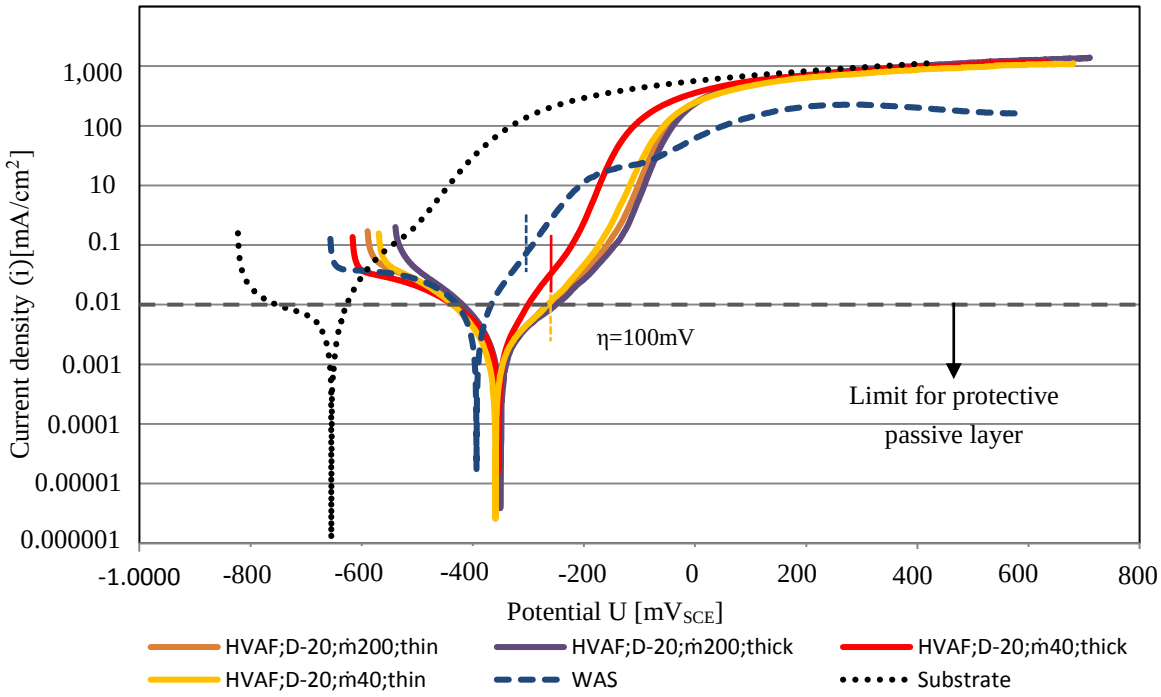

Figure 40: Potentiodynamic polarization plots of the fine powder HVAF and WAS coatings

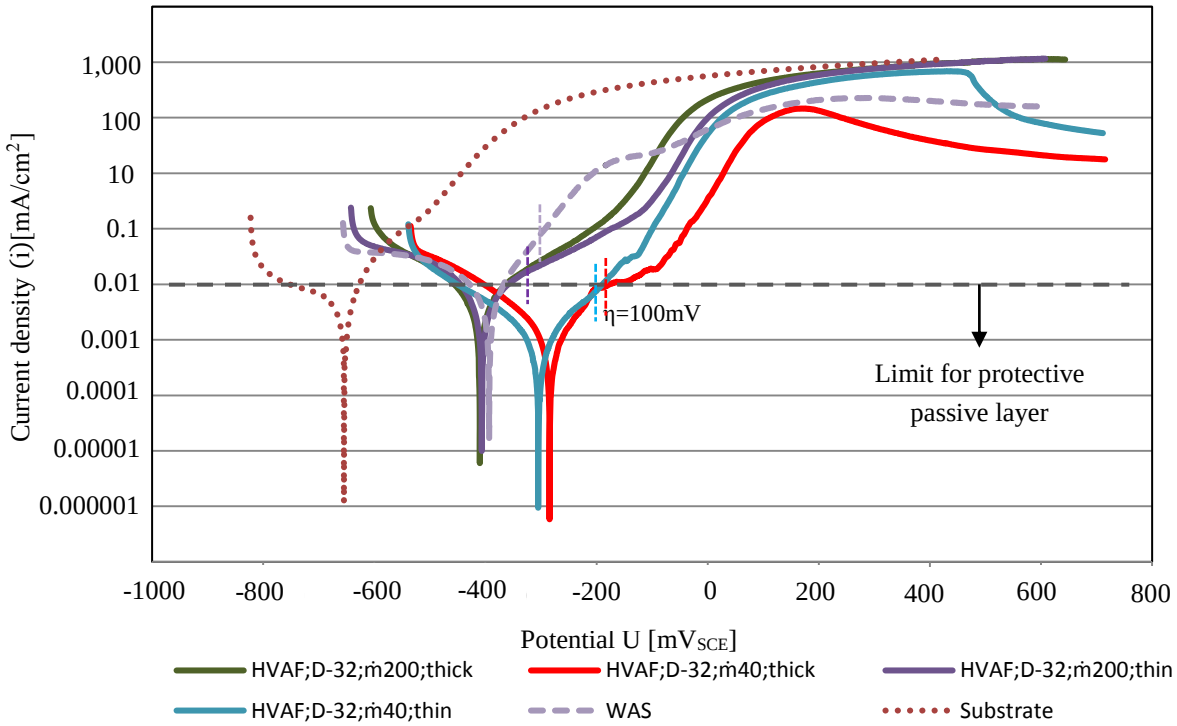

Figure 41: Potentiodynamic polarization plots of the coarse powder HVAF and WAS coatings

Table 9: Electrochemical values of polarization test

Sample	Corrosion current density ($\mu A/cm^2$)	Rest potential U_R [mV_{SCE}]
D-32, ṁ40, thick	0.554	-284.6
D-32, ṁ40, thin	0.983	-305.1
D-32, ṁ200, thick	1.566	-410.1
D-32, ṁ200, thin	1.325	-406.4
D-20, ṁ40, thick	1.577	-353.8
D-20, ṁ40, thin	1.336	-359.3
D-20, ṁ200, thin	1.961	-355
D-20, ṁ200, thick	1.884	-350.5
WAS	5.466	-393.3
Substrate	3.98	-654.7

It was expected that fine powder fraction (-20+3µm) coatings provide better chemical resistance due to the higher ratio of surface to volume which leads to the higher melting degree. Higher melting degree provides more available heat energy per particle, which generates denser microstructure with homogeneous splat boundaries. However, for the ṁ40 g/min coatings the result was completely opposite; coarse powder had a higher rest potential and lower current density (in the other cases, the current densities are in the same range). For better interpretation, further analysis such as SEM are required. By considering same overpotential (η=100mV) from the rest potential, D-32;ṁ: 40 coatings remained below the passive limit line, which states adequate performance of passive protection layer. In addition, their anodic branch curves increased very slowly, which indicate the formation of corrosion products that inhibit the flow of current. On the contrary, coatings with narrow passive region and high slop of anodic branch such as D-32; ṁ200 or D-20;ṁ40;thick passed the passivation limit .This negative behavior is presumably due to the insufficient protective chromium oxide layer in the coatings. Fig.42,43 show the cross-section of coated samples after corrosion test. Pictures confirm mentioned claims that lower powder feed rate coatings

have a better corrosion resistance with lower corrosion depth. It is worth saying that in the most cases the corroded layers have a homogeneous distribution near the top layer.

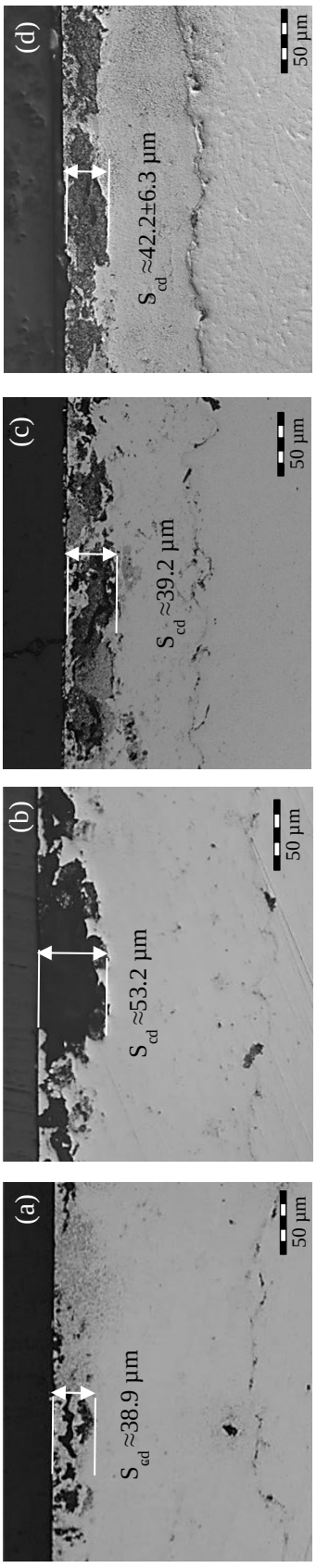

Figure 42:Cross-sections of D-32 coatings after corrosion test of (a) Thick, ṁ40 (b) Thick, ṁ200 (c) Thin, ṁ40 (d) Thin, ṁ200

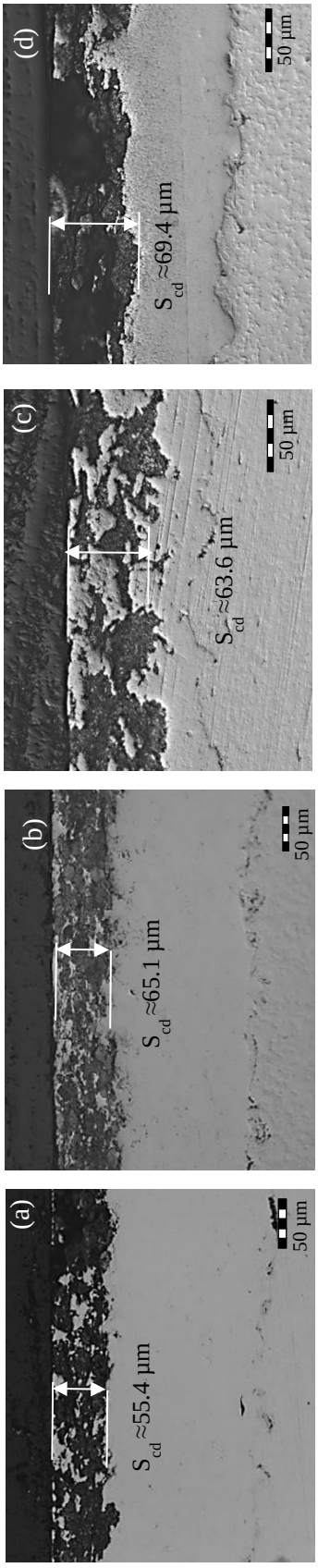

Figure 43:Cross-sections of D-20 coatings after corrosion test of (a) Thick, ṁ40 (b) Thick, ṁ200 (c) Thin, ṁ40 (d) Thin, ṁ200

The corrosion resistance of the WAS coating is inferior as compared to the HVAF coatings due to the higher amount of porosity which leads to the easy penetration of chloride ions. Another reason for the lower rest potential and higher current density of the WAS coating may be due to the higher oxygen content with respect to the HVAF coatings. Metal oxides are formed between partially molten particles during spraying process. These metal oxides not only hinder the formation of dense passive film but also become the diffusion channels for electrolyte to cause inner corrosion. As a result, there are corrosion products in deeper layers (Fig.44). In addition, in all HVAF and WAS samples there were not under corrosion regions which show adequate protection over substrate. Fig.44 compares the optical microscopy images of the corroded cross sections of different coatings after polarization in 5% NaCl aqueous solution as well as small pictures of sample's surfaces in which the corroded regions are indicated by arrows.

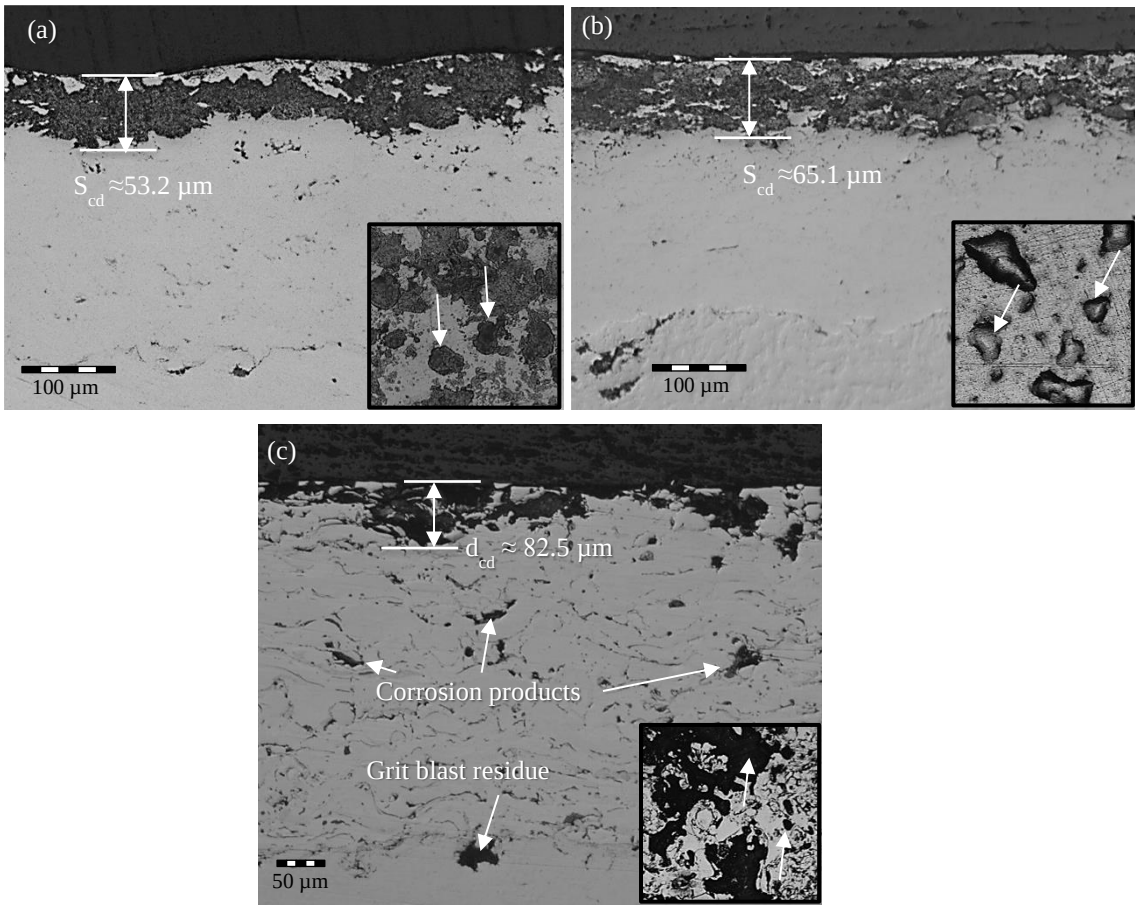

Figure 44: Comparison of corroded sample's cross-section and surface of WAS and HVAF coatings: (a) D-32; ṁ200; thick, (b) D-20; ṁ200; thick, (c) WAS

4.3.2 Aging investigation

For the qualitative surface consideration, samples were removed from furnace after 100 hours. Fig.45 shows their pictures. After aging, the substrate exhibited strong surface corrosion which means that steel substrate had weak protection against test condition. For the other coatings, selective and crevice corrosion were observed. As it clear in the pictures, the crevice corrosion could only be observed at the edges due to the small crevice between sealing ring and surface. The protection for the WAS coating was weaker respect to the HVAF coatings based on the more selective corrosion signs. The cross-section pictures after aging experiment in Fig.46,47 confirm that there was no surface corrosion in the HVAF coatings. The arrows indicate a few number of corroded regions. Moreover, in all coatings there was no evidence of under corrosion at the interface of surface and coating.

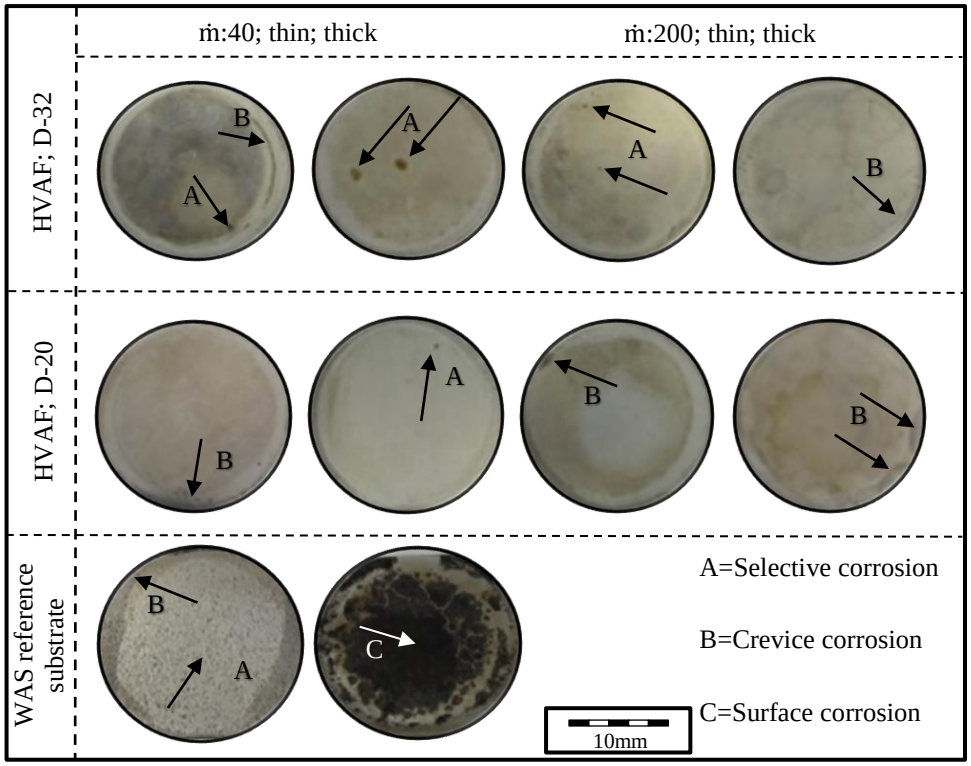

Figure 45: pictures of aged samples after 100 hours in saturated steam of 0.5% NaCl-solution at 110°C

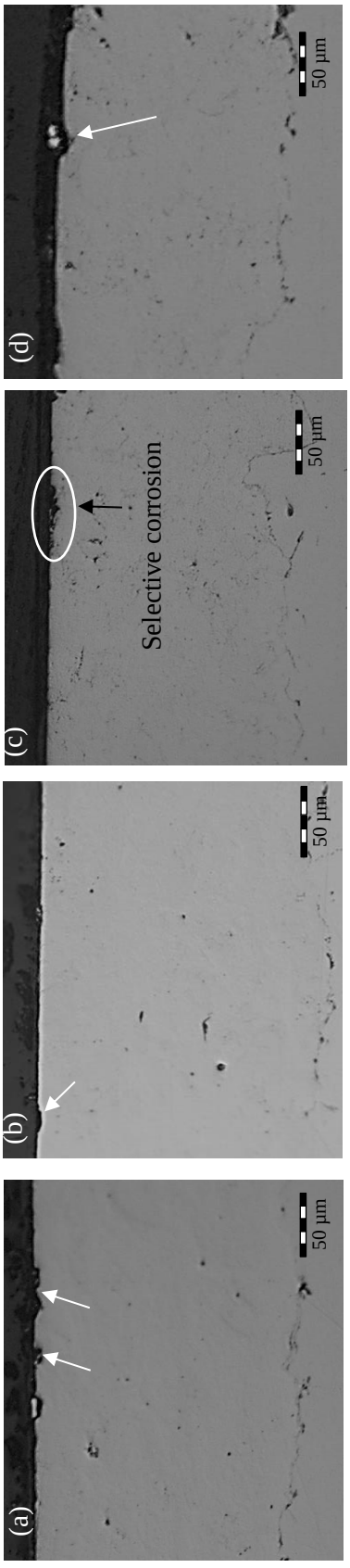

Figure 46: Cross-sections of D-32 coatings after aging test (a) Thick, ṁ40 (b) Thick, ṁ200 (c) Thin, ṁ40 (d) Thin, ṁ200

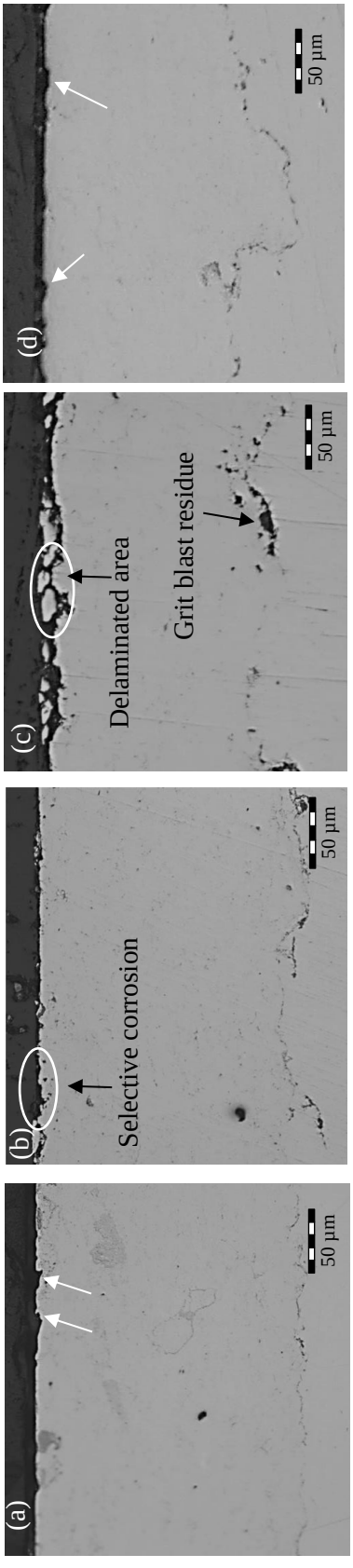

Figure 47: Cross-sections of D-20 coatings after aging test (a) Thick, ṁ40 (b) Thick, ṁ200 (c) Thin, ṁ40 (d) Thin, ṁ200

Fig.48 compares the cross-section pictures of the reference and HVAF coating after aging test. As it shown, the surface of WAS coating corroded more than the HVAF coating due to the decrease of cohesion of coating after aging (as it explained in part 4.2.3.2).

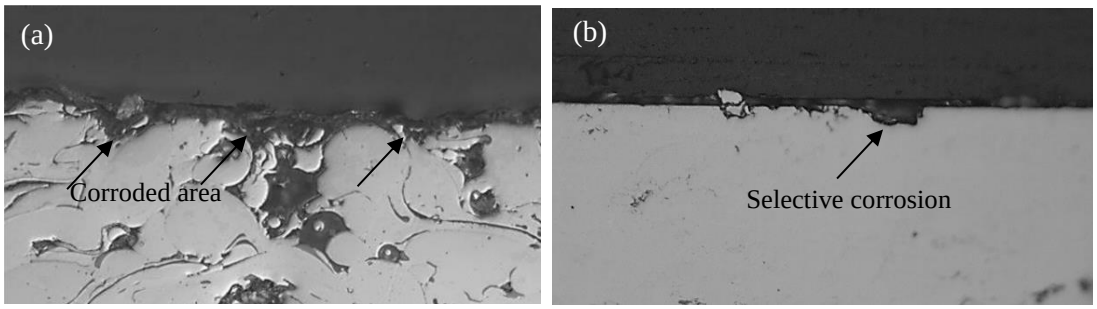

Figure 48: The cross-section pictures after aging experiment (a) WAS coating, (b) HVAF; D-32,ṁ200

Chapter 5

Conclusion

In this current research, the novel High Velocity Air Fuel (HVAF) process was utilized to develop a cost-efficient, wear and corrosion protection Fe-based coating system which offers comparable protection to an industrially established noble Fe-based coating systems produced by wire-arc-spraying (WAS). Therefore, coatings with two thicknesses (140 µm and 250 µm), powder fractions of -20 +3 µm and -32 +11 µm and powder feed rates of ṁ40 g/min and ṁ200 g/min were produced. Subsequent, characterization, mechanical and corrosion properties of the coating system were investigated and compared to the sealed FeCrBMnSiC WAS-sprayed reference coating system. The conclusions resulting from the investigation are summarized as follows:

- Produced coatings had a dense, crack free microstructure with low oxide content and good bonding to the substrate with respect to the fairly porous structure of the WAS coating with micro-crevices around splats. The surface roughness Ra as well as thickness of the HVAF samples were significantly lower compared to the WAS sample which can result in lower time consuming post-production, saving feedstock materials and less thermal insulation effect. In addition, finer powder fraction (- 20+3 µm) was able to produce smoother surface.
- The XRD-analysis indicated that there is no detectable change of phases in the HVAF coatings, compared with the same materials in the form of powders and the detected phase was FeCrB with peak angles of 43.2°, 44.7° and 56.3°.
- The microhardness of the HVAF coatings were considerably higher than substrate and reference coating which resulted in high fracture toughness. Moreover, higher powder feed rate of the HVAF sprayed coatings provided higher fracture toughness with shorter crack length.

- There was significant improvement of wear resistance for all the HVAF coatings under considered testing conditions in comparison to the substrate and the WAS coating, independent of the powder fraction and the powder feed rate. The improvement was due to a number of reasons, including: low amount of porosity and oxides in microstructure, increase in microhardness and formation of hard boride phases. Furthermore, the wear coefficient of coatings slightly increased after aging test due to formation of corrosion products.
- Either of the HVAF coatings provided a superior corrosion behavior compared to the substrate and the reference coating as indicated by a higher corrosion potential, lower passive current density and wider passive region. The improvement of corrosion properties of the HVAF coatings was due to the significant reduction of defects such as porosity, micro-crevices, and splat boundaries. Among the HVAF samples, the coatings produced with lower powder feed rate (40g/min) exhibited lower corrosion current density as well as lower corrosion depth. For moderate overpotential (100mV), the course powder fraction coatings (-32 +11 µm) showed better corrosion behavior until the breakthrough based on the slight slope of anodic branch. Moreover, no under-corrosion was detected for all investigated HVAF coatings.
- Developed coating system was protective against aging test and only some surface regions corroded. In addition, electrolyte could not reach the substrate at high temperature to produce under corrosion area.

Therefore, the HVAF-sprayed FeCrB coating system is superior as compared to the sealed WAS FeCrBMnSiC coating in terms of corrosion and wear resistance, microstructure and mechanical properties. Considering this improvement, such coating system could offer a cost-effective alternative to the WAS-sprayed Fe-based coating systems for large area application.

Suggestions for future work

- Investigation of the corrosion properties of HVAF coatings by means of the other corrosion techniques such as salt spray test
- Investigation of thermal conductivity of produced coatings to evaluate a thermal efficiency

- Further analysis, e.g. SEM/EDS to the corroded samples to define produced corrosion products
- Assessment of developed residual stresses in the coatings since they have remarkable effects on the tribological properties

Chapter 6

References

1. Papp, J.F., et al. , *Factors that influence the price of Al, Cd, Co, Cu, Fe, Ni, Pb, rare Earth elements and Zn: Open-File Report*. 2008.
2. Wu, J.B., and J. Redman. , *Hardfacing with cobalt and nickel alloys.* Welding Journal, 1994. **73.9**.
3. Suh, M., et al., *Inhalation cancer risk assessment of cobalt metal* Regulatory Toxicology and Pharmacology 2016. **79** p. 74-82.
4. Xie, H., et al., *The cytotoxicity and genotoxicity of soluble and particulate cobalt in human lung epithelial cells.* Environmental and molecular mutagenesis 2016. **57.4** p. 282-287.
5. D. Lison, C., in: G.F. Nordberg, B.A. Fowler, M. Nordberg, *Handbook on the Toxicology of Metals.* Elsevier Academic Press,, 2015. **Vol. II Specific Metals, 4th ed.**: p. 745–764.
6. Rausch, S., et al. , *Influence of Machine Hammer Peening on the Tribological Behavior and the Residual Stresses of Wear Resistant Thermally Sprayed Coatings.* Procedia CIRP 45, 2016: p. 275-278.
7. Liu, W.-H., Fuh-Sheng Shieu, and Wei-Tien Hsiao, *Enhancement of wear and corrosion resistance of iron-based hard coatings deposited by high-velocity oxygen fuel (HVOF) thermal spraying.* Surface and Coatings Technology 2014. **249** p. 24-41.
8. Zhang, H., et al. , *The effect of high-velocity oxy-fuel spraying parameters on microstructure, corrosion and wear resistance of Fe-based metallic glass coatings.* Journal of Non-Crystalline Solids, 2014. **406**: p. 37-44.
9. Ma, H.R., et al. , *Wear resistance of Fe-based amorphous coatings prepared by AC-HVAF and HVOF*. Materials Science and Technology, 2017. **33.1**: p. 65-71.
10. Chen, S.-y., et al., *Investigation of competing failure mechanism and life of plasma sprayed Fe-based alloy coating under rolling–sliding contact condition.* Tribology International 2016. **101**: p. 25-32.
11. Sigolo, E., et al. , *Wear resistant coatings of boron-modified stainless steels deposited by plasma transferred arc.* Surface and Coatings Technology, 2016. **302** p. 255-264.
12. Ulutan, M., et al. , *Microstructure and wear behaviour of plasma transferred arc (PTA)-deposited FeCrC composite coatings on AISI 5115 steel.* Materials Processing Technology, 2016. **236** p. 26-34.
13. Wang, W., et al. , *Enhancement of oxidation and wear resistance of Fe-based amorphous coatings by surface modification of feedstock powders.* Materials & Design, 2015. **73** p. 35-41.

14. Bobzin, K., et al. , *Process development for innovative iron alloy metallic glass coatings.* Advanced Engineering Materials, 2016. **18.10**: p. 1833-1840.
15. Wang, H.Q., et al. , *Microstructure and mechanical properties of molybdenum–iron–boron–chromium cladding using argon arc welding.* Materials Science and Technology, 2016. **32.16** p. 1694-1701.
16. Guo, W., et al. , *Fabrication and characterization of Fe-based amorphous coatings prepared by high-velocity arc spraying.* Materials & Design, 2015. **78** p. 118-124.
17. Cheng, J.B., et al., *Microstructure and mechanical properties of FeBSiNb metallic glass coatings by twin wire arc spraying.* Journal of thermal spray technology, 2013. **22.4** p. 471-477.
18. Li, R., et al. , *Microstructure and high-temperature oxidation behavior of wire-arc sprayed Fe-based coatings.* Surface and Coatings Technology 2014. **251** p. 186-190.
19. Liang, X.B., et al. , *Erosion properties of Fe based amorphous/nanocrystalline coatings prepared by wire arc spraying process.* Surface Engineering, 2010. **26.3**: p. 209-215.
20. Lima, C.R.C., et al. , *Assessment of abrasive wear of nanostructured WC-Co and Fe-Based coatings applied by HP-HVOF, flame, and wire arc spray.* Journal of thermal spray technology, 2014. **23.7**: p. 1097-1104.
21. Liu, X.Q., et al. , *Microstructure and properties of Fe-based amorphous metallic coating produced by high velocity axial plasma spraying.* Journal of Alloys and Compounds 2009. **484.1-2**: p. 300-307.
22. Zhang, H., et al., *Effect of feedstock particle sizes on wear resistance of plasma sprayed Fe-based amorphous coatings.* Surface and Coatings Technology 2014. **258** p. 495-502.
23. Zeng, Z., et al. , *Effects of some light alloying elements on the oxidation behavior of Fe and Ni-Cr based alloys during air plasma spraying.* Journal of thermal spray technology 2010. **19.1-2** p. 128-136.
24. Guo, R.Q., et al., *Study of structure and corrosion resistance of Fe-based amorphous coatings prepared by HVAF and HVOF.* Corrosion Science 2011. **53.7** p. 2351-2356.
25. Bolelli, G., et al. , *Tribological behavior of HVOF-and HVAF-sprayed composite coatings based on Fe-Alloy+ WC–12% Co.* Surface and Coatings Technology 2014. **248** p. 104-112.
26. Zhang, C., et al. , *Wear behavior of HVOF-sprayed Fe-based amorphous coatings.* Intermetallics 2012. **29** p. 80-85.
27. Wang, Y., et al. , *Corrosion and erosion–corrosion behaviour of activated combustion high-velocity air fuel sprayed Fe-based amorphous coatings in chloride-containing solutions.* Corrosion Science, 2015. **98** p. 339-353.
28. Guo, R.Q., et al. , *Corrosion and wear resistance of a Fe-based amorphous coating in underground environment.* Intermetallics 2012. **30** p. 94-99.
29. Bobzin, K., Öte, M., Knoch, M.A. and Sommer, J,, *Influence of powder feed rate on corrosion and wear properties of Fe-based HVAF coatings.* Proc. 20. WTK-Werkstofftechnisches Kolloquium, 2018.
30. Bobzin K, Ö.M., Knoch M A , Sommer J, *Development of HVAF-sprayed novel Fe-based coatings for large area applications* Proceedings of ITSC 2017 p. 339-45.
31. Vuoristo, P., and Per Nylén. , *Industrial and research activities in thermal spray technology in the Nordic region of Europe.* Journal of Thermal Spray Technology 2007. **16.4**: p. 466-471.

32. Tenkula, J., Bjarne Hellman, and Jorma Majava, *Yankee cylinder with a plasma-sprayed carbide coating*. 1992. p. 152.
33. Ghosh, A.K., *Fundamentals of paper drying–theory and application from industrial perspective.* Evaporation, Condensation and Heat Transfer, 2011. **InTech**.
34. Vuoristo, P., *Thermal spray coating processes.* 2014: p. 229-276.
35. Bolelli, G., et al. , *Tribology of HVOF-and HVAF-sprayed WC–10Co4Cr hardmetal coatings: a comparative assessment.* Surface and Coatings Technology, 2015. **265** p. 125-144.
36. Hulka, I., et al. , *Comparison of structure and wear properties of fine-structured WC-CoCr coatings deposited by HVOF and HVAF spraying Processes.* Solid State Phenomena, 2012. **188**(Trans Tech Publications).
37. Hashmi, S., *Comprehensive materials processing.* Newnes, 2014.
38. G. Bolelli, I.H., H. Koivuluoto, L. Lusvarghi, A. Milanti, K. Niemi, P. Vuoristo, *Properties of WC–FeCrAl coatings manufactured by different high velocity thermal spray processes.* Surf. Coat. Technol. 247, 2014: p. 74–89.
39. Halling, J., *Introduction: Recent Development in Surface Coating and Modification Processes.* MEP, London, 1985.
40. Majumdar, J.D., and I. Manna, *Laser surface engineering of titanium and its alloys for improved wear, corrosion and high-temperature oxidation resistance.* Laser Surface Engineering, 2015: p. 483-521.
41. Davis, J.R., ed. , *Surface engineering for corrosion and wear resistance.* ASM international, 2001.
42. Fauchais P.L, H.J.V., Boulos M.I, *Combustion Spraying Systems, Thermal Spray Fundamentals.* Springer, 2014: p. 227-303.
43. Davis, J., *Handbook of Thermal Spray Technology, ASM International Materials Park, OH, 2004.*
44. Tucker Jr, R.C., *Introduction to Coating Design and Processing* ASM Handbook 2013. **5** p. 76-88.
45. Pawlowski, L., *The science and engineering of thermal spray coatings*. 2008: John Wiley & Sons.
46. James Maurice Boileau, T.J.P., Paul George Sanders, Matthew John Zaluzec, Pravansu Sekhar Mohanty, Vikram Varadarrajan *Composite Metal Alloy Material*. 2013, Ford Global Technologies LLCUniversity of Michigan
47. Walser, B., *The importance of thermal spray for current and future applications in key industries.* Spraytime, 2004. **10**(4): p. 1-7.
48. Herman, H., S. Sampath, and R. McCune, *Thermal spray: current status and future trends.* MRS bulletin, 2000. **25**(7): p. 17-25.
49. Dorfman, M.R., *Thermal spray coatings.* Handbook of Environmental Degradation of Materials (Third Edition), 2018: p. 469-488.
50. Hedges, M.K., A. P. Newbery, and P. S. Grant. , *Characterisation of electric arc spray formed Ni superalloy IN718.* Materials Science and Engineering: A 326.1, 2002: p. 79-91.
51. Watanabe, T., Tadayuki Sato, and Atsushi Nezu. , *Electrode phenomena investigation of wire arc spraying for preparation of Ti-Al intermetallic compounds.* Thin Solid Films 407.1-2, 2002: p. 98-103.
52. Gedzevicius, I., and A. V. Valiulis. , *Analysis of wire arc spraying process variables on coatings properties.* Journal of Materials Processing Technology 175.1-3 2006: p. 206-211.

53. Steffens, H.-D., Z. Babiak, and M. Wewel., *Recent developments in arc spraying.* IEEE Transactions on Plasma Science 18.6, 1990: p. 974-979.
54. Guillen, D.P., and Brian G. Williams. , *Oxidation behavior of in-flight molten aluminum droplets in the twin-wire electric arc thermal spray process*. 2005, Idaho National Laboratory (INL).
55. Hussary, N.A. 1999, University of Minnesota.
56. Marantz, D.R., and Daniel R. Marantz., *State of the art arc spray technology.* Thermal Spray Research and Applications, 1990: p. 113.
57. Lester, T., and Stuart Milton. , *Metallized coatings application: an overview of the flame-and arc-spraying processes used for surface finishing.* metal finishing 103.7-8 2005: p. 35-38.
58. Pourmousa, A., et al., *Particle diagnostics in wire-arc spraying system.* ITSC 2004: International Thermal Spray Conference 2004: Advances in Technology and Application, 2004.
59. Pourmousa, A., J. Mostaghimi, A. Abedini, and S. Chandra, *Particle Size Distribution in a Wire-Arc Spraying System.* Journal of Thermal Spray Technology, December 2005. **14**(4).
60. Wire-Arc Manual, S.-M., Westbury, NY.
61. Hasan, M., *High velocity oxy-fuel (HVOF) thermal spray deposition of functionally graded coatings.* 2005.
62. Stokes, J., *Production of coated and free-standing engineering components using the HVOF (High Velocity Oxy-Fuel) process*, in *School o f Mechanical and Manufacturing Engineering*. 2003, Dublin City University.
63. Rakhes, M., *Laser Surface Modification of HVOF Coatings for Improvement of Corrosion and Wear Performance*, in *Faculty of Engineering and Physical Science*. 2013, The University of Manchester (United Kingdom).
64. Sunde, A., *Properties of thermal sprayed coatings for internal use in pipes and bends*. 2015, MS thesis. NTNU.
65. *Alternatives Werkstoffkonzept zur umweltfreundlichen Herstellung von Aluminium*. 12. September 2018: Fraunhofer-Institut für Fertigungstechnik und Angewandte Materialforschung IFAM, Institutsteil Dresden.
66. Fedrizzi, L., et al. , *Corrosion and wear behaviour of HVOF cermet coatings used to replace hard chromium.* electrochimica acta 49, 2004. **17-18**: p. 2803-2814.
67. Berce, A., *Simulation of thermal spraying in IPS virtual paint*, in *Department of Applied Mechanics, Division of Fluid Mechani*. 2011, CHALMERS UNIVERSITY OF TECHNOLOGY.
68. S. Kuroda, Y.T., H. Yumoto, S. Taira, H. Fukanuma, *Peening action and residual stresses in hvof thermal spraying of 316l stainless steel* Proceedings of fifteenth international thermal spray conference, 1998: p. 569–574.
69. Zhang, S.J.H., and D. G. McCartney, *Microstructure formation and corrosion behaviour in HVOF-sprayed Inconel 625 coatings.* Mater. Sci. Eng. A, 2003. **344**(1-2): p. 45–56.
70. Wang Q, Z.S., Cheng Y and Xiang J, *Wear and corrosion performance of WC-10Co4Cr coatings deposited by different HVOF and HVAF spraying processes.* Surface & Coating Technology 2013. **218**: p. 36-127.
71. Björklund, C.L.a.S., *Internal Diameter HVAF Spraying for Wear and Corrosion Applications.* Thermal Spray Technology, 2015. **vol. 24**: p. pp. 235–243.

72. Berger, L.-M.P., Roberto & Spatzier, Jörg & Matthews, Steven, *Potenzial von HVAF-Spritzprozessen; Potential of HVAF Spray Processes.* Thermal Spray Bulletin, 2013. **6**: p. 16-20.
73. W.J.Trompetter, A.M., M.Hyland, *Role of oxides in high velocity thermal spray coatings.* Nuclear Instruments and Methods in Physics Research B, 2002. **190**: p. 518–523.
74. C.Lyphout, S.B., M.Karlsson, M.Runte, G.Reisel, and P.Boccaccio, *Screening Design of Supersonic Air Fuel Processing for Hard Metal Coatings.* Thermal Spray Technology, 2014. **23**(8): p. 1323–1332.
75. Y.-Y. Wang, C.-J.L., and A. Ohmori, *Examination of factors influencing the bond strength of high velocity oxy-fuel sprayed coatings.* Surfuce and Coating Technology, 2006. **200**(9): p. 2923–2928.
76. Zheng, S.L.L.a.X.P., *Microstructure and properties of AC-HVAF sprayed Ni60/WC composite coating.* Alloys and Compounds, 2009. **480**(2): p. 254–258.
77. Zeng, Z., et al., *Structure and corrosion behavior of 316L stainless steel coatings formed by HVAF spraying with and without sealing.* Surface and Coatings Technology, 2008. **203**(3-4): p. 284-290.
78. Liu, S., et al., *The influence of HVAF powder feedstock characteristics on the sliding wear behaviour of WC–NiCr coatings* Surface and Coatings Technology, 2008. **202**(20): p. 4893-4900.
79. Verstak, A., *Kermetico High Velocity Air-Fuel Thermal Spray*. March 2017, www.kermetico.com.
80. Molins, R., et al. , *Interlamellar boundary characterization in Ni-based alloy thermally sprayed coating.* Materials Science and Engineering, 2003. **A 351**(1-2): p. 325-333.
81. Shi, D., Mingheng Li, and Panagiotis D. Christofides, *Diamond jet hybrid HVOF thermal spray: rule-based modeling of coating microstructure.* Industrial & engineering chemistry research 2004. **43.14**: p. 3653-3665.
82. Knight, R.W.S.R., and Ronald W. Smith *Thermal spray forming of materials.* Powder Metal Technologies and Applications, 1998. **7** p. 408-419.
83. Magnani, M., et al., *Influence of HVOF parameters on the corrosion and wear resistance of WC-Co coatings sprayed on AA7050 T7.* Surface and Coatings Technology, 2008. **202**(19): p. 4746-4757.
84. Schwenk, A., *HVOF-K2 spraying of iron-based alloys for applications in the printing industry.* Colloquium High Speed Flame Spraying, 8, Cold Spraying: Equipment + Applications, HVOF Spraying Conference, 8, 2009.
85. Osamanda, A., Battenbough, A. and Staines, A., *Maßgeschneiderte HVOF-Beschichtungssyteme auf Fe-Cr und Fe-Cr-Ni Basis für den Verschleiß- und Korrosionsschutz.* Thermal Spray Bulletin 2, pp. 117/22, 2012.
86. Katranidis, V., et al. , *Experimental study of high velocity oxy-fuel sprayed WC-17Co coatings applied on complex geometries. Part A: influence of kinematic spray parameters on thickness, porosity, residual stresses and microhardness.* Surface and Coatings Technology 2017. **311**: p. 206-215.
87. K. Bobzin, M.Ö., M.A. Knoch, J. Sommer, *Influence of grain size on the corrosion/wear behaviour of HVAF sprayed Fe-based coatings*, in *International thermal spray conference and exposition*. 2018: Orlando, Florida.
88. Gui, M., et al. , *Influence of processing parameters on residual stress of high velocity oxy-fuel thermally sprayed WC-Co-Cr coating.* Journal of materials engineering and performance 2012. **21.10**: p. 2090-2098.

89. Smith, M.F., et al, *A comparison of techniques for the metallographic preparation of thermal sprayed samples.* Journal of Thermal Spray Technology 2.3, 1993: p. 287-294.
90. Brundle, C.R., et al., *Encyclopaedia of Materials Characterization.* Manning Publications Company, Greenwich, ISBN No 0750691689, 1992.
91. Mitutoyo, *Jis b 0601, geometric product specification (gps) - surface texture: profile method.* 2001.
92. Fu, S., et al., *A non-contact measuring system for in-situ surface characterization based on laser confocal microscopy.* Sensors 2018. **18.8**: p. 2657.
93. Cullity, B., D., *Elements of X-Ray Diffraction* Addison-Wesley, USA, ISBN No 0201610914, 1978.
94. Touloukian, Y.S., et al. , *Thermal expansion: nonmetallic solids.* Thermophysical Properties of Matter, 1977. **13**: p. 1270-1272.
95. Handbook, A., *Mechanical Testing*. 1985, The Materials Information Society, ISBN No 0871700077. p. Vol.8.
96. *ASTM1421-99, ASTM C 1421-99 Standard Test Methods 15.01*. 1999.
97. A.C.Fischer-Cripps, B.R.L., *Indentation stress-strain curves for "quasi-ductile" ceramics.* Acta Materialia, Volume 44, Issue 2, 1996: p. 519-527.
98. Cook, R.F., and George M. Pharr., *Direct observation and analysis of indentation cracking in glasses and ceramics.* Journal of the American Ceramic Society, 1990. **73.4**: p. 787-817.
99. Chicot, D., et al, *Vickers Indentation Fracture (VIF) modeling to analyze multi-cracking toughness of titania, alumina and zirconia plasma sprayed coatings.* Materials Science and Engineering, 2009. **A 527.1-2**: p. 65-76.
100. Bhushan, B., and Gupta, B K, *Handbook of Tnbology Material Coating and Surface Treatments.* McGraw-Hill, New York, 1991.
101. Papadopoulos P, P.M., Rainforth W M, *Investigation of fundamental wear mechanisms at the piston ring and cylinder wall interface in internal combustion engines.* Proceedings of the Institution of Mechanical Engineers, Part J: Journal of Engineering Tribology, 221(3), 2007: p. 333-343.
102. *NTNU, Wear, lecture notes.* 2014.
103. (Ed.), K.G.B., *Surface Engineering for Wear Resistance.* Prentice Hall, New Jersey, 1988.
104. *Astm, A. S. T. M. G99: Standard Test Method for Wear Testing with a Pin-on-Disk Apparatus, ASTM Stand, 2010, P.1-5.*
105. Wang, W.-S., et al., *Real-time telemetry system for amperometric and potentiometric electrochemical sensors.* 2011. **Sensors 11.9**: p. 8593-8610.
106. G. Bolelli, B.B., J. Laurila, L. Lusvarghi, A. Milanti, K. Niemi, P. Vuoristo, *Micromechanical properties and sliding wear behaviour of HVOF-sprayed Febased alloy coatings.* Wear 276–277, 2012: p. 29–47.
107. Zhao, L.L., E. , *Influence of the spraying processes on the properties of 316L stainless steel coatings.* Surf. Coat. Technol., 2003. **162**: p. 6–10.
108. Redjdal, O.Z., B.; Tabti, M.S.; Henda, K.; Lacaze, P.C. , *Characterization of thermal flame sprayed coatings prepared from FeCr mechanically milled powder.* Mater. Process. Technol., 2013. **213**: p. 779–790.
109. Zhao, W.M.W., Y.; Dong, L.X.; Wu, K.Y.; Xue, J. , *Corrosion mechanism of NiCrBSi coatings deposited by HVOF.* Surf. Coat. Technol., 2005. **190**: p. 293–298.

110. Milanti, A., et al. , *Microstructure and sliding wear behavior of Fe-based coatings manufactured with HVOF and HVAF thermal spray processes.* Journal of Thermal Spray Technology, 2016. **25.5**: p. 1040-1055.
111. P. Vuoristo, S.A., S. Tuurna, T. Mäntylä, E. Cordano, F. Fignino, G.C. Gualco, *Development of HVOF sprayed NiCoCrAlYRe coatings for use as bond coats of plasma sprayed thermal barrier coatings.* International Thermal Spray Conference, 2002. **6** p. 470–475.
112. Sadeghimeresht, E.M., N.; Nylén, P.; Björklund, S., *Corrosion performance of bi-layer Ni/Cr2C3-NiCr HVAF thermal spray coating.* Appl. Surf. Sci, 2016. **369**: p. 470–481.
113. Bobzin, K., M. Öte, and T. Königstein. , *Manufacture of iron-based, amorphous coatings with high fracture toughness,* in *IOP Conference Series: Materials Science and Engineering*. 2017, IOP Publishing.
114. Liang, K.M., G. Orange, and G. Fantozzi., *Evaluation by indentation of fracture toughness of ceramic materials.* Journal of Materials Science 1990. **25.1**: p. 207-214.
115. Liu, Y., Traugott E. Fischer, and Andrew Dent. , *Comparison of HVOF and plasma-sprayed alumina/titania coatings_microstructure, mechanical properties and abrasion behavior.* Surface and Coatings Technology, 2003. **167.1**: p. 68-76.
116. Glancy, S.D., *Preserving the M icrostructure o f Thermal Spray Coatings.* Journal o f Advanced M aterials and Processes, Vol. 148, Issue 1, pp. 37-40, 1995.
117. Glancy, S.D., *Pursuit of a Universal Metallographic Procedure for Thermally Sprayed Coatings.* Proceedings o f the 8th N ational Thermal Spray Conference, Texas, USA, 1995: p. pp. 493-498.
118. N. Briks, G.H.M.E., *Introduction to High Temperature Oxidation of Metals.* Edward Arnold (Publishers) Ltd, London 1983: p. 32.
119. B., S., *Linerless Eutectic Al-Si Engine Wear.* Microstructural Evolution, 2009: p. 10-81.
120. Maksud Helali, M., *Spray forming of thin walled net-shaped components of hard materials by high velocity oxy-fuel thermal spraying process*. 1994, Dublin City University.

Appendices

Appendix I

Samples preparation steps

- Cutting

First step is cutting and is necessary when investigated component is too large to handle. During a sectioning, debonding of coating and over-heating of a sectioned surface should be avoided. Selection of a rate of cutting as well as cut-off blade are crucial which generally depend on the material to be sectioned. In Table10, various types of cut-off blades were shown. [116]

Table 10: various types of cut-off blades

Disk	Application
B250	For high-speed steels, heat-treated steels, non-corrosive steels
C300	Universal wheel for materials of high to very high hardness
D300	Universal wheel for medium hard materials, case-hardened steels
E300	For soft steels, non-ferrous materials, plastics
F250/F300	For titanium and titanium alloy
H300	For case-hardened and medium hard materials
I300	For construction steels and cast materials
60A30	Very hard ferrous metals

- Mounting

Next step is mounting which consist of two techniques; hot-compression mounting and cold-castable mounting. In the first one the sample which set in thermoplastic or thermoset resin subjected to elevated temperature (140-200 °C) and high pressure (20-40 MPa) for less than 15 minutes. In cold-castable mounting which is carried out in vacuum, sample is cured in epoxy at 80 °C for 60 minutes[117].

- Grinding

Next step of metallurgical preparation is grinding. To do so, the manual machine was used with silicon carbide papers. The roughness of papers starts from 180 and goes through 400, 600, 800 and 1200. The coarse papers were used to remove the damage experienced during sectioning and the fine papers were used to removal of the deformation experienced during grinding with coarse papers. Each paper was used for about 4 minutes.

- Polishing

Polishing is an essential step in preparation to achieve mirror like and highly reflective surface. It helps to remove deformations included during grinding, besides remove all smears from surface. Polishing with diamond abrasives is very effective and sufficient to prepare a coating. In the current work, diamond polishing was done at 3 and 1 microns respectively.

Wear mechanisms

1. Chemical and oxidative

The chemical and oxidative wear occurs due to reactions happening on wearing surfaces is any environment. These chemical reactions take place between worn material and a corroding medium, which can be a chemical reagent, reactive lubricant or even air. Oxidative wear happens when worn surface reacts with the oxidizing environment at room or high temperature in dry conditions [118, 119].

2. Erosion wear

Erosion usually is produced by the repeated impingement of sharp and small hard particles and leads to progressive material loss and occasionally roughening of the exposed surface. Different parameters can affect the erosion rate such as the number, direction, and velocity of the particles striking the surface. Erosion wear can accelerate by corrosion when the media is corrosive. Hence, by application of a hard coating along with improved corrosion resistance, it is possible to improve erosion-resistance property [103, 119].

3. Fatigue wear

When a surface of a component, subjected to severe contact forces and repeated stress cycling. These repeating stresses in a rolling or sliding contact lead to fatigue failure and cracking. From the maximum shear stress point, crack for failure will initiate and move nearer to the surface. Since the shear stress is maximum below the surface in a pure rolling contact, subsurface and surface fatigue wear are the influential failure modes in rolling element bearing [63, 120].

4. Fretting wear

Fretting is a type of interactive wear that takes place with small relative vibratory movements at high frequency are applied on component. Fretting wear is initiated by adhesion and is amplified by corrosion. Thus, the role of environment is strong in this mode. Fretting typically occurs in stationary joints that are fixed by bolts, pins, rivets, or other mechanisms, and also at the various contact points in antifriction, or rolling-element and bearings. In other word, nonrotating antifriction bearings that are subject to vibration for a while may have fretting wear [120].

Appendix II

Pictures of equipment

Figure 49: Cutting machine

Figure 50: Confocal laser scanning microscope

Figure 51: Vickers microhardness instrument

Figure 52: Fischerscope instrument

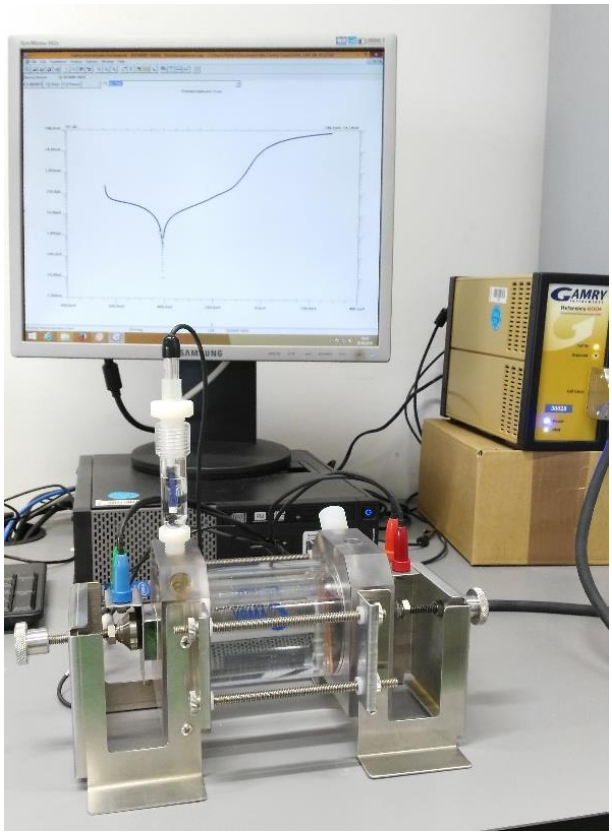

Figure 53: Polarization test setup

Figure 54: Pin-on-Disk instrument